ABSTRACT

A Microwave Radiometer System for Use in Biomedical Applications

Laura R. Ballew

Mentor: B. Randall Jean, Ph.D.

The biomedical industry is a rapidly growing sector and demands are increasing for the production of safe and noninvasive technologies. With the current surge of diabetes, a very desirable application for these technologies is a non-invasive monitor for blood glucose level. Recently, microwave sensing has offered hope for safer diagnostic and therapeutic procedures. One specific sensing technique involves a microwave radiometer, which provides a purely passive measurement of naturally emitted electromagnetic radiation from material objects. A highly sensitive receiver, the radiometer can detect radiation for the purpose of obtaining useful information about a particular object, thus providing a safe tool for the biomedical industry.

This thesis outlines the microwave properties of radiometry and presents the design of a microwave radiometer aimed at biomedical applications. Experimental results demonstrate the applicability and repeatability of the device, as well as its performance as a biomedical sensor.
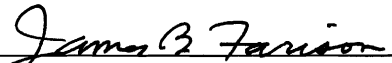
A Microwave Radiometer System for Use in Biomedical Applications

by

Laura R. Ballew, B.S.

A Thesis

Approved by the Department of Electrical and Computer Engineering

_____
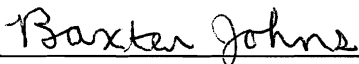
James B. Farison, Ph.D., Chairperson

Submitted to the Graduate Faculty of
Baylor University in Partial Fulfillment of the
Requirements for the Degree
of
Master of Science in Biomedical Engineering

Approved by the Thesis Committee

_____

B. Randall Jean, Ph.D., Chairperson

_____

Carolyn T. Skurla, Ph.D.

_____

Baxter Johns, Ph.D.

Accepted by the Graduate School
December 2006

_____

J. Larry Lyon, Ph.D., Dean

TABLE OF CONTENTS

LIST OF FIGURES

LIST OF TABLES

LIST OF SYMBOLS AND ABBREVIATIONS

AC – alternating current

A/D – analog to digital

AF – audio frequency
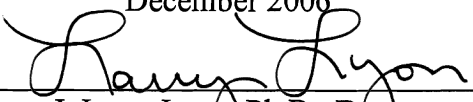
B – bandwidth

B_f – blackbody spectral brightness

c – speed of light ($3 \times 10^8 ms^{-1}$)

Cd – detector sensitivity

CT – computed tomography

D – electric flux density

dBm – decibels relative to one milliwatt

DRO – dielectric resonator oscillator

E – electric field

e – emissivity

f – frequency

G – gain

h – Planck's constant (6.63×10^{-34} J·s)

IF – intermediate frequency

k – Boltzmann's constant (1.38×10^{-23} J/K)

K – Kelvin

LO – local oscillator

MRI – magnetic resonance imaging

NF – noise figure

op amp – operational amplifier

P – power

PIN – p-type intrinsic n-type

R – distance from radiometer to object being measured

RF – radio frequency

SMA – SubMiniature version A

SPDT – single-pole double-throw

T_A – antenna temperature

T_B – brightness temperature

T_N – noise temperature

T_R – reference temperature

V_d – detector voltage

V_{out} – output voltage

VSWR – voltage standing wave ratio

δ – penetration depth

ε – permittivity (dielectric constant)

ε_r – relative permittivity

ε_0 – permittivity of free space (8.85×10^{-12} F/m)

ε_w – dielectric constant of pure water

ε_{w0} – static dielectric constant of water

$\varepsilon_{w\infty}$ - high frequency limit of ε_w

$\varDelta T$ – radiometer sensitivity

$\varDelta G$ – gain variation

λ – wavelength

μ – permeability

ω – angular frequency

σ – conductivity

σ^2 – variance

σ_{out} – output standard deviation

$\varTheta$ – viewing angle

τ – integration time

ACKNOWLEDGMENTS

I would like to thank Dr. Jean for his gracious help and encouraging words throughout the duration of my project. Thank you to my parents, who have so selflessly given their support, both in undergraduate and graduate work. I also wish to thank my brother, Brett, who has always believed in me and encouraged me. I will always look up to you. Finally, I wish to thank my husband, Matt, who has been by my side from the beginning. I am so thankful for your love, prayers, patience, and your belief in my ability to succeed.

DEDICATION

To my two favorite engineers, my dad and my husband.

CHAPTER ONE

Introduction

Microwave sensing has played an expanding role in the world's technological

advances over the past fifty years [1]. From radar to radiometry, microwave sensing has

been used for an increasing number of applications, including ground mapping, soil

moisture determination, thermography, and breast cancer detection [2]. With the ability

to safely penetrate many kinds of media (e.g. clouds or biological specimens), microwave

sensors find a significant place among other modalities of measurement.

Microwave radiometry is an important branch of microwave sensing because it

provides a passive sensing technique for detecting naturally emitted electromagnetic

radiation. A microwave radiometer is the device used to conduct radiometric

measurements and is the focus of this research. While the radiometer has been a

significant research instrument for atmospheric and earth surface evaluations, the device

lends itself to further exploration of passive measurements, especially in the biomedical

realm [3]. With increasing demands for safety, radiometers may present an alternative

solution in the biomedical field for areas such as diagnostics and monitoring during

therapy. For example, radiometers are being researched for tumor detection applications,

including brain cancer and thyroid cancer detection, which would offer a noninvasive

substitute to the current computed tomography (CT) and magnetic resonance imaging

(MRI) technologies [4, 5]. Microwave radiometry allows greater penetration depth in

tissues because it uses lower frequencies than similar infrared procedures [2]. Since

1

radiometers have excellent sensitivity and penetration depth, they are also being studied for noninvasive temperature monitoring in biological tissues such as the human brain [6, 7]. This research presents radiometry as a noninvasive monitoring technique during hypothermia treatment in newborns. During this treatment, the newborns' heads are cooled to provide neural protection after hypoxia ischemia, a deficiency in blood flow that hinders oxygen needed for the brain [8]. Current brain temperature monitoring tools are invasive, requiring measurements through the nasal cavity or ear, for example. Radiometry eliminates the need for invasive tools and provides a more comfortable monitoring technique [6, 7].

One specific need, and a strong motivation for this research, has emerged as a result of the growing number of those living with diabetes. The disease is marked by high levels of glucose resulting from insulin defects. In 2002, diabetes was considered the fifth deadliest disease and 7% of the nation's population had been diagnosed with it [9]. Diabetics must monitor their blood glucose level daily to maintain a healthy lifestyle. Since current invasive methods require a blood sample for glucose determination, it is fitting that research should follow a path leading toward noninvasive monitoring. Some noninvasive methods exist, such as implantable glucose sensors and monitors that extract fluid through the skin [10]. Although more attractive than finger pricking, these methods cause skin irritations and adverse reactions from the body's immune system. They also are not completely noninvasive because they require frequent calibration through finger pricking. Another noninvasive procedure known as near-infrared (NIR) spectroscopy injects a beam of near-infrared light through the skin [10]. A spectroscopy monitor detects the absorption intensity of the energy being sent through

the skin. With this technique, glucose signals are small and are often masked by noise [10]. From a sensing-method point of view, radiometers present an ideal solution for blood glucose monitoring because of their inherent passive, and in effect, noninvasive operation. In other words, no energy is injected into the body while making measurements, and thus, any fear of electromagnetic radiation effects on the body is nullified. Also, radiometers have the ability to detect extremely small signals that are otherwise obstructed by noise.

This research focuses on the design and implementation of one such radiometer, which will be used in this study to produce accurate and repeatable measurements for a variety of biomedical experiments, including a blood glucose monitoring application.

CHAPTER TWO

Microwave Radiometry

Microwave Properties

Electromagnetic waves surround us and cover an extensive range of frequencies from DC (0 Hz) to 10^{25} Hz. Within this known spectrum are radio waves, visible light, x-rays, gamma rays, and cosmic rays, among other sources of electromagnetism. The microwave portion of the spectrum is considered to range from approximately 100 MHz to 300 GHz, a subset of the radio spectrum (see Figure 1).
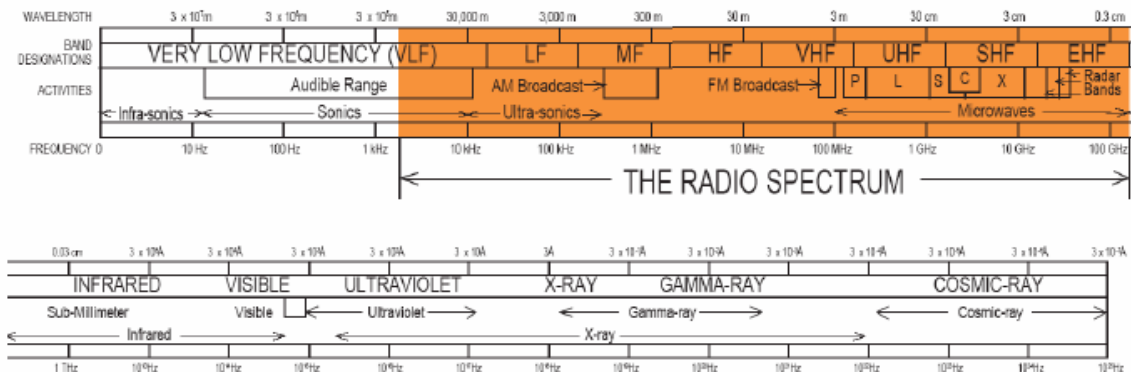
Figure 1: The electromagnetic spectrum [11]

Depending upon measurement objectives, microwave radiometers can be designed for any specific frequency range in the microwave spectrum. Radiometers use passive sensing, while other microwave sensors, such as radar, use active sensing. A passive sensor is simply a receiver whereas an active sensor employs a receiver and transmitter.

All forms of matter are composed of atoms that can be further divided into protons, neutrons, and electrons. The electrons oscillate and emit energy in the form of thermal radiation. Therefore, all matter, from soil to atmospheric elements to biological specimens, absorb and emit electromagnetic radiation [12]. Electromagnetic absorption translates to heat and an object's temperature rises in accordance with its absorption. This heat is then emitted from the object, thus keeping it in a state of thermal equilibrium with its surroundings [1]. It is this noise-like emitted radiation that radiometers can detect for the purpose of determining an object's microwave properties. Since the radiometer is an extremely sensitive receiver, it can exploit the fact that different objects emit a broad assortment of frequencies and intensities of radiation [13]. The power, P, emitted by an object with ideal absorbing and ideal emitting characteristics can be related to the physical temperature, T, of the object by

$$P = kTB, \tag{1}$$

where k is Boltzmann's constant (1.38×10^{-23} J/K) and B is the radiometer bandwidth in Hertz [1]. Such an object is known as a blackbody, which maintains thermal equilibrium by absorbing and emitting energy at the same rate [14]. For radiometric purposes, the term brightness temperature, T_B, is used to describe the intensity of radiation emission. It is defined by the formula

$$T_B = \frac{P}{kB}, \tag{2}$$

and is related to the physical temperature of an object through a parameter known as emissivity (e), given by

$$e = \frac{T_B}{T} \ [15]. \tag{3}$$

Emissivity expresses the amount of radiation emitted by an object relative to the amount of radiation emitted by a blackbody at the same temperature [12]. A blackbody's emissivity is denoted as 1 and is dimensionless, while non-ideal bodies have an emissivity in the range of $0 \leq e \leq 1$ [14]. Therefore, no real body can emit more energy than a blackbody [12]. Substituting T_B from equation (3) into equation (2) indicates that the emitted power for all non-blackbody radiation is

$$P = ek TB. \tag{4}$$

Equation (3) assumes a homogeneous body with uniform temperature. In reality, objects have rough surfaces, varying temperatures, and are non-homogeneous. Any discontinuities in the surface can cause emitted radiation to scatter in many different directions from the medium, as illustrated in Figure 2 below. Figure 3 demonstrates that the brightness temperature is also a combination of directional radiation from within the medium [1]. According to data from Ulaby, *et al.*, an increase in surface roughness results in an increase in emissivity [16].
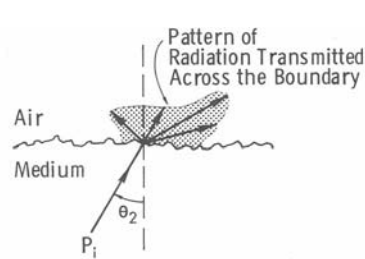
Figure 2: Emission from a rough surface [1]
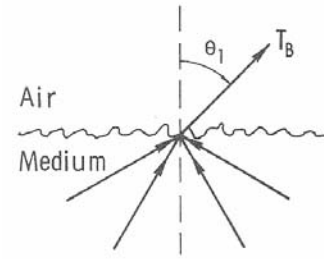
Figure 3: Brightness temperature composed of contributions from many directions [1]

A radiometer's antenna senses the brightness temperature of objects, which translates to the antenna temperature, T_A. This quantity is considered to be the power measured by the radiometer. A more formal definition by states that the antenna temperature is "the temperature to which the radiation resistance of the antenna must be

raised in order to produce the same noise power as that contributed by the various sources

observed by the antenna" [17].

A blackbody emits radiation independently of direction according to Planck's

blackbody radiation law,

$$B_f = \frac{2hf^3}{c^2}\left(\frac{1}{e^{\frac{hf}{kT}}-1}\right), \text{ [1]}$$
(5)

where

B_f = blackbody spectral brightness ($Wm^{-2}sr^{-1}Hz^{-1}$)
h = Planck's constant (6.63×10^{-34} J·s)
f = frequency (Hz)
k = Boltzmann's constant
T = absolute temperature (K)
c = velocity of light (3×10^8 ms^{-1}).

The Planck radiation curves in Figure 4 below reveal that the maximum spectral

brightness at any given frequency increases with temperature [1]. Overall, more radiation

is emitted at higher frequencies as temperature rises [12].
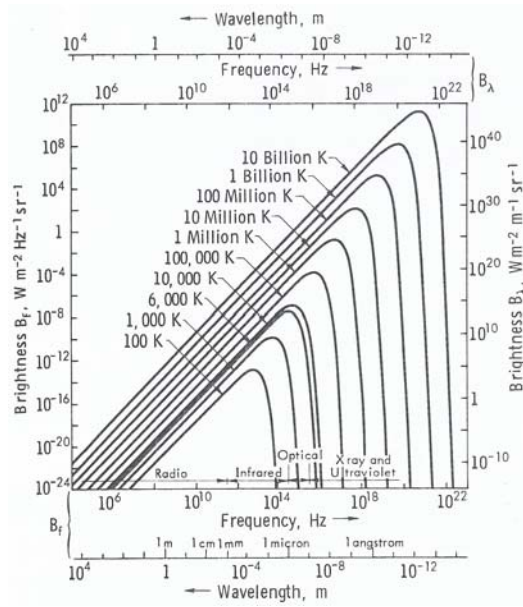
Figure 4: Planck radiation-law curves [1]

Two different approximations to Planck's radiation law exist: the Wien radiation law and the Rayleigh-Jeans law [1]. The Wien radiation law approximates the high frequency portion of Planck's law, assuming that $hf/kT \gg 1$. Therefore,

$$\frac{1}{e^{\frac{hf}{kT}} - 1} \cong \frac{1}{e^{\frac{hf}{kT}}} = e^{-\frac{hf}{kT}} \, , \qquad (6)$$

reduces (5) to

$$B_f = \frac{2hf^3}{c^2} e^{-\frac{hf}{kT}} \text{ [1].} \qquad (7)$$

For the low frequency approximation, the Rayleigh-Jeans law assumes that hf/kT<<1, which is used in the Taylor series expansion of

$$e^x - 1 = \left(1 + x + \frac{x^2}{2} + \cdots\right) - 1 \cong x \text{ for } x \ll 1. \qquad (8)$$

Substituting this approximation into (5) yields

$$B_f = \frac{2f^2 kT}{c^2} = \frac{2kT}{\lambda^2} \, , \qquad (9)$$

which is a simple, yet accurate, representation of Planck's law. Comparisons of Planck's law with its two approximations are illustrated in Figure 5 below. The Rayleigh-Jeans approximation deviates from Planck's law by less than 1 percent up to approximately 117 GHz. This result makes the approximation useful for most of the microwave portion of the spectrum including that used in this research [1].
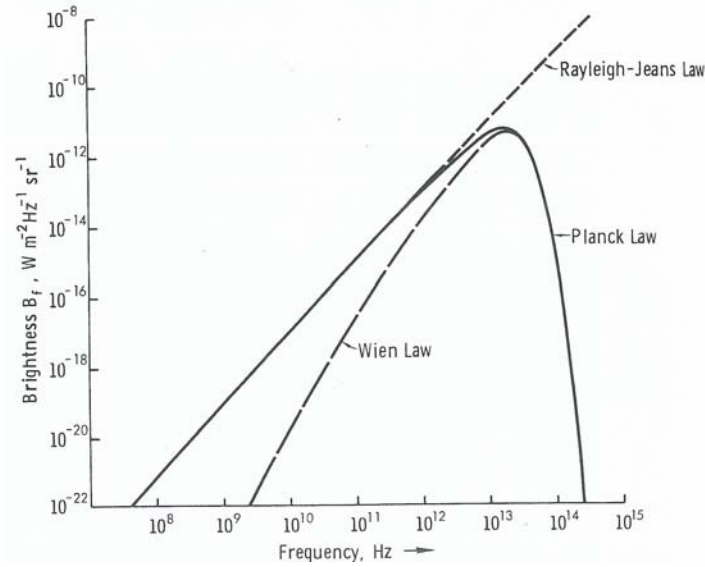
Figure 5: Comparison of Planck's law with its low-frequency (Rayleigh-Jeans law) and high-frequency (Wien's law) approximations at 300 K [1]

The correspondence between power and temperature can be explained by considering an antenna placed in an absorptive medium at temperature T (see Figure 6 below). Assuming a lossless antenna with a purely resistive impedance equal to the load impedance, a direct correlation can be made between a transmission line terminated with a resistive load and a transmission line terminated in a matched antenna. Therefore, when in thermal equilibrium, the temperature of the matched termination must equal the temperature of the medium for a perfectly absorbing medium [17].
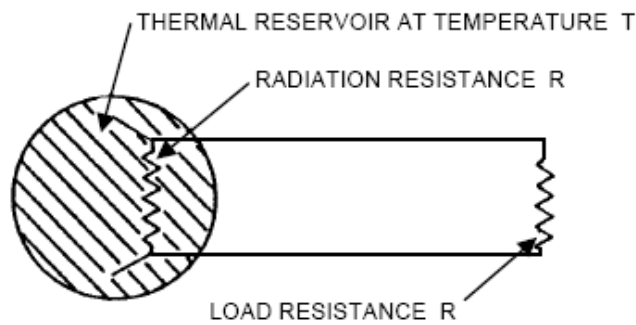
Figure 6: Equivalent circuit of an antenna immersed in an absorbing medium at temperature T [17]

Similarly, if the antenna is enclosed in a blackbody at temperature *T*, then the emitted

power is equal to the power emitted by a resistor at the same temperature, assuming that

both are matched to a receiver with bandwidth *B* [1]. The power is defined in equation

(1) and demonstrated in Figure 7 below.
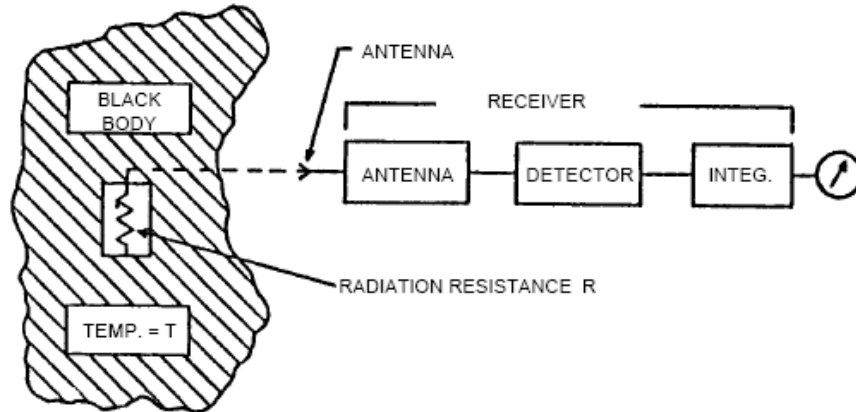
Figure 7: Simplified block diagram of an antenna and receiver [17]

A detailed derivation of the correspondence between power and temperature is given by

Ulaby, *et al*. [1].

Radiometers detect noise-like signals, including both the desired signal from the

object under observation and the unwanted noise emitted by the intervening propagation

medium and system components. For radiometers, the desired signal may be on the order

of -90 decibels relative to one milliwatt (dBm), or 10×10^{-10} milliwatts (mW). It is

essential to distinguish between the two signals to acquire useful information about a

particular object [14]. Undesired noise is a result of electrons moving in random motion,

causing electric charge and voltage fluctuations [1]. Radiometer sensitivity, which

defines the smallest change in temperature that the radiometer can detect, is affected by

the undesired noise. An ideal radiometer with gain G and bandwidth B measures an output power of

$$P=kBGT_A. \tag{10}$$

A noise temperature, T_N, is an additive factor in real systems, so equation (10) becomes

$$P=kBG(T_A+T_N) . \tag{11}$$

According to Ulaby, *et al.*, radiometer sensitivity can be described as the standard deviation of the output [1]. The input signal to the radiometer is depicted as having zero mean with a variance. Integrating the input signal of bandwidth B over time τ reduces its variance by a factor of $B\tau$ [16]. The equation

$$\sigma^2 \cong \frac{P^2}{B\tau} \tag{12}$$

describes the variance and also the standard deviation if a square root is applied. After the signal propagates through the detection phase (to be described in detail in the section *Types of Radiometers*), the voltage is equal to the detector sensitivity multiplied by the RF gain and the total input noise power. The total output voltage is then related to the detector output voltage by

$$V_{out} = g_{LF}V_d , \tag{13}$$

with g_{LF} as the low pass filter voltage gain [16]. This equation relates the output voltage to the input power and also to the standard deviation, given by the square root of equation (12). Therefore, the equation

$$\frac{\sigma_{out}}{V_{out}} = \frac{1}{\sqrt{B\tau}} \tag{14}$$

indicates the ratio of the output's standard deviation to the output voltage. Equating this to temperature characterization produces

$$\frac{\Delta T}{T} = \frac{1}{\sqrt{B\tau}}, \tag{15}$$

where T is equal to $T_A + T_N$ from equation (11) and ΔT is the standard deviation of the

system temperature [16]. This is the radiometer sensitivity formula, which is more

commonly written as

$$\Delta T = \frac{T_A + T_N}{\sqrt{B\tau}}. \tag{16}$$

Here, T_A represents the radiometer input temperature, T_N is the noise temperature, B is the

bandwidth before detection, and τ is the integration time [3].

In addition to the inherent signal noise, gain fluctuations caused by instability

within the amplifiers can play a role in the radiometer's sensitivity [18]. The error due to

gain fluctuations is described by the formula

$$\Delta T_G = (T_A + T_N)\frac{\Delta G}{G}, \tag{17}$$

where $\Delta G/G$ is the system gain variation . Most radiometer systems require a sensitivity

of 1 K or less, which is achieved by means described in Chapter Three.

Types of Radiometers

Total Power

The total power radiometer is one of three main types. Although this type of

radiometer is not as common as the others, it is simpler and serves to explain the basics of

radiometer systems. Figure 8 below is a block diagram that illustrates a typical total

power radiometer with a superheterodyne front end. The superheterodyne configuration

adds a mixer, local oscillator (LO), and intermediate frequency (IF) filters and amplifiers.

Most of the gain is added in the IF section. The mixer serves to convert the radio

frequency (RF) to a convenient IF frequency. A band pass (or low pass in some cases)

filter, known as the IF filter, suppresses out-of-band noise. The square-law detector

produces an output voltage proportional to the input power. In the words of Leinweber,

"the DC component of diode output is proportional to the square of the input AC voltage"

[19]. Square-law detectors are rated with a sensitivity constant that is usually expressed

in millivolts per milliwatt. Signal fluctuations are smoothed by the integrator, which acts

as a low pass filter and determines the integration time. The integrator has been an

analog configuration, such as an RC low pass filter, in classic radiometer systems. With

the overwhelming increase in microprocessor design and implementation, the digital

integrator has increased in popularity [20].
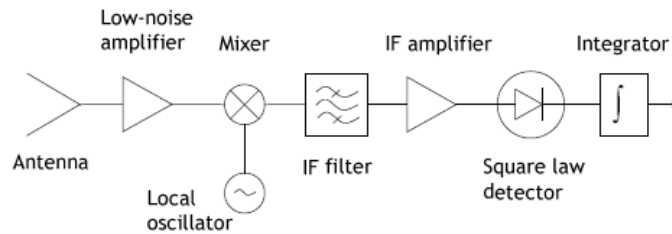
Figure 8: Block diagram of total power radiometer [18]

The total power radiometer's sensitivity is calculated with equation (16), and the detector

output voltage is as described in *Microwave Properties*. Therefore, there is a dependence

of the output voltage upon the receiver noise temperature and gain [1]. Gain fluctuations

are detrimental to a radiometer's performance; thus, the total power radiometer is an

impractical tool for most radiometric applications.

Dicke Radiometer

In 1946, R.H. Dicke solved the problem of gain fluctuations by adding a reference load that supplied a differential measurement for the radiometer (see Figure 9). A switch, later known as a Dicke switch, was employed to switch the input between the antenna and a reference load. This technique can also be thought of as rapidly and repeatedly calibrating the radiometer [14].
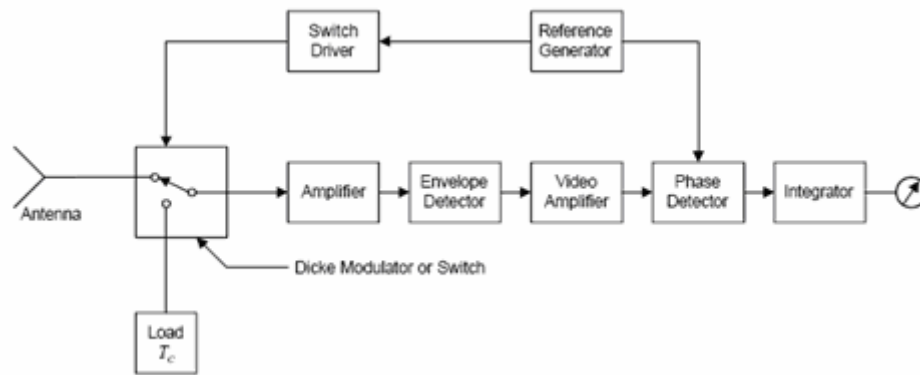
Figure 9: Block diagram of Dicke radiometer [17]

In addition to the total power radiometer, the Dicke radiometer includes a synchronous detector on the square-law detector output that multiplies the signal by +1 or -1, depending on the switch's position [3]. Multiplying the signal transforms it into a DC signal to be fed into the analog-to-digital (A/D) converter. The signal is switched quickly enough so that the system's gain remains constant over one full switching cycle. Therefore, the gain for each half-cycle (one half-cycle being the period at which the switch is positioned on the antenna and the other half-cycle being the period at which the switch is positioned on the reference load) is identical. In effect, the output voltages of each half-cycle are

$$V_A = C_d GkB(T_A + T_N) \tag{18}$$

and

$$V_R = C_d GkB(T_R + T_N) \tag{19}$$

where C_d is a constant and T_R is the reference noise temperature. After the synchronous detector and low pass filter, the output voltage becomes

$$V_o = \tfrac{1}{2}\, G(T_A\text{-}T_R), \tag{20}$$

demonstrating that the output voltage is differential and independent of receiver noise temperature (T_N) [1]. Since the antenna temperature is observed only half of the time, the sensitivity of the Dicke radiometer is reduced by a factor of 2 from the total power radiometer, giving

$$\Delta T = 2\frac{T_A + T_N}{\sqrt{B\tau}}\,. \tag{21}$$

Even with this degradation in sensitivity, the Dicke radiometer is the most popular type of radiometer because of its superior ability to minimize gain fluctuations [3].

Noise-Injection Radiometer

The noise-injection radiometer is similar to the Dicke radiometer, with the addition of a variable noise generator. Referring to equation (20), if the antenna temperature and reference temperature are equal, then the output of the Dicke radiometer is zero. A loop in the noise-injection radiometer acts to maintain this condition by adjusting the noise input that is added to the antenna temperature. The sensitivity

$$\Delta T = 2\frac{T_R + T_N}{\sqrt{B\tau}} \tag{22}$$

is very similar to that of the Dicke radiometer and the output is independent of gain and noise temperature fluctuations [3].

Other Radiometer Types

In addition to the three most common types of radiometers, other types continue to be developed. For example, the correlation radiometer is a multichannel device that measures two brightness temperatures and the correlation between them. Variations of the correlation radiometer exist, such as the polarimetric radiometer, which measures horizontal and vertical brightness temperatures and finds the correlation (known as Stokes parameters) between them. A synthetic aperture radiometer takes the product of antenna pairs and measures the signal using a basic correlation radiometer. The use of antenna pairs can improve spatial resolution without involving a single large antenna, making this radiometer useful for remote sensing in space [20]. Still other radiometer types have been designed and are explained in more detail by Skou [20].

CHAPTER THREE

Microwave Properties of Biological Substances

A comprehensive knowledge of the microwave properties associated with biological substances must be gained for purposes of designing an appropriate biomedical radiometer. These properties form the building blocks of this research and aid in providing a set of specifications for the radiometer.

Permittivity and Water

Biological substances are comprised mostly of water. Given the fact that water covers over two-thirds of the earth's surface and constitutes 72% of the human body, it is only natural that the focus of determining biological properties would fall upon this substance [21]. A key measurement parameter for microwave properties is permittivity, or dielectric constant, which is directly related to water content. Different biological tissues have different water contents; hence, the permittivity varies among tissues [22-24]. The permittivity explains a material's energy storage and loss characteristics when placed in an electric field. Because of their polar nature, water molecules attempt to align themselves within the presence of an electric field. Permittivity describes how easily the alignment is achieved and it is calculated by the equation

$$\varepsilon = \frac{D}{E} \quad ,$$

(23)

where D is the electric flux density and E is the electric field strength [13]. Water is considered to be a dispersive medium because of its frequency dependence of

permittivity [13, 23, 24]. At low frequencies water molecules easily align with an

applied electric field, thereby creating a large induced polarization. As frequency

increases, the field varies too quickly for the molecules to align, causing the induced

polarization to be less. When the frequency of the applied field approaches the resonant

frequency of the molecule, losses caused by the rotation effects are increased. The

reduced polarization effect means that permittivity decreases with frequency. Losses that

are due to conductivity decrease with increasing frequency. Figure 10 below illustrates

the dependence of the real part of the permittivity upon frequency for some biological

tissues.
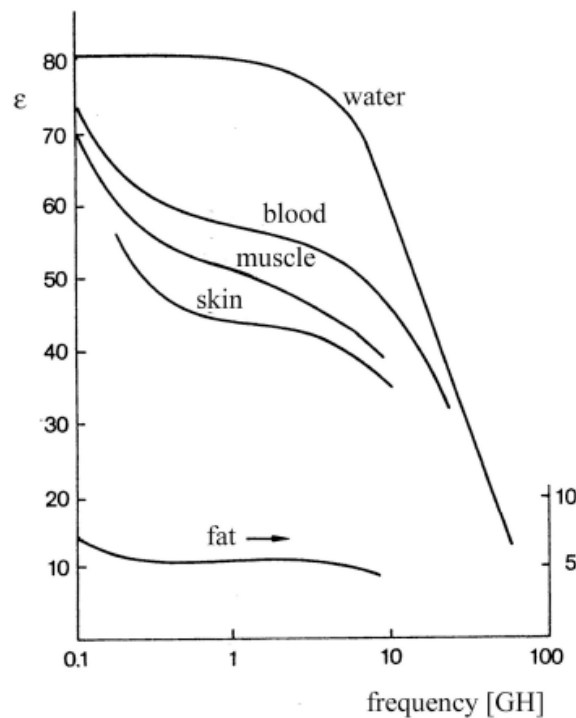
Figure 10: Relative dielectric constant versus frequency for various tissues [2]

Even though biological tissues carry a resemblance to water, their electrical behavior is

strikingly complex. Extensive research on this subject has led to the development of

mathematical models to explain the behavior of biological tissues by portraying their

dielectric spectra [23, 24, 26]. Their frequency dependence, otherwise known as

dispersion, is modeled by the Debye equation:

$$\hat{\varepsilon} = \varepsilon_\infty + \frac{\varepsilon_s - \varepsilon_\infty}{1 + j\omega\tau}. \qquad (24)$$

In this equation, the static ($\omega\tau \ll 1$) dielectric constant is ε_s, the high frequency limit of

$\hat{\varepsilon}$ ($\omega\tau \gg 1$) is ε_∞, and τ is the relaxation time [15, 23]. An alternative to the Debye

equation is the Cole-Cole equation:

$$\hat{\varepsilon}(\omega) = \varepsilon_\infty + \sum_n \frac{\Delta\varepsilon_n}{1 + (j\omega\tau_n)^{(1-\alpha_n)}} + \frac{\sigma_i}{j\omega\varepsilon_0}, \qquad (25)$$

which describes the dielectric behavior for multiple dispersions of a biological tissue

[23]. Figure 11 further highlights the complexity of biological tissues, evident from the

step-like behavior of tissue permittivity as a function of frequency. The figure reveals the

four distinct dispersion regions for biological tissues: α-dispersion, β-dispersion, δ-

dispersion, and γ-dispersion [23, 24].
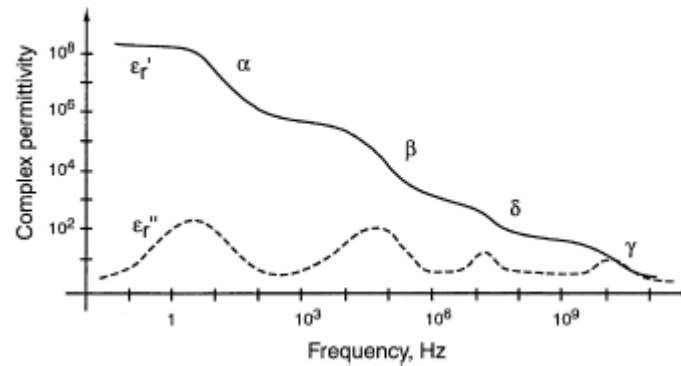
Figure 11: Idealized dispersion regions for tissue [26]

Interestingly, the α-dispersion region consists of remarkably high dielectric constant values. This phenomenon is caused by interfacial polarizations, or Maxwell-Wagner polarizations, that create charge buildup on the cell membrane [26-28]. At higher frequencies (radio frequencies), β-dispersion occurs as a result of cell membranes resembling short circuits. In this case, permittivity becomes representative of the main electrolyte that fills cells and the space around them. Since this electrolyte is comprised of water and ions, the permittivity of biological tissues begins to mirror that of water [27, 28]. The δ-dispersion region represents the effects of protein bound water, which contributes to about 10% of the water content in tissues [26, 29]. The term "bound" is derived from the fact that water's ability to align with the electric field has been impeded by its position and contact with proteins. This hindrance causes the relaxation frequency to decrease 50 to 100 times from that of free water [27, 29]. The final relaxation and the source of γ-dispersion occurs at approximately 10 GHz as a result of unbound water [24, 27]. Of these dispersions, the latter three are the most important for this research because they represent the effects of bound water and free water relaxation.

An important relationship exists between permittivity and emissivity that serves to further explain the electrical properties of biological tissues [22]. The relationship is expressed through Fresnel's equations:

$$e_H(\Theta) = 1 - \left| \frac{\cos\Theta - \sqrt{\varepsilon_r - \sin^2\Theta}}{\cos\Theta + \sqrt{\varepsilon_r - \sin^2\Theta}} \right|^2 \qquad (26)$$

and

$$e_V(\Theta) = 1 - \left| \frac{\varepsilon_r \cos\Theta - \sqrt{\varepsilon_r - \sin^2\Theta}}{\varepsilon_r \cos\Theta + \sqrt{\varepsilon_r - \sin^2\Theta}} \right|^2 . \qquad (27)$$

Here, Θ is the viewing angle and the portions inside the absolute value signs represent the reflectivity for horizontal and vertical polarization [30]. Consequently, emissivity also depends on water content, but inversely from the correlation between permittivity and water content.

Permittivity and Blood Glucose

It is necessary to expand research from general biological tissues to blood glucose properties if the radiometer is to perform as a glucose sensor. Limited research is available for the correlation between permittivity and blood glucose level. Despite this scarcity, current research suggests that a relationship is evident, which offers hope for the radiometer's ability to detect blood glucose level changes.

Nikawa *et al.* demonstrated a change in permittivity related to glucose level *in vitro* by measuring the resulting transmission coefficient of varying glucose solutions. The authors varied the amount of glucose solution placed into an acrylic resin container [31]. The results suggest the possibility of noninvasive glucose determination, but it is far from determining a passive, noninvasive solution for measuring glucose *in vivo*.

Park *et al.* produced encouraging results for measuring permittivity changes according to glucose level in a hamster [32]. The authors fed sugar water to the hamster and measured permittivity over time at 10 kHz after placing a sample cell on the hamster's tail. For comparison, glucose data was also taken with a glucose monitor during the experiment. The results imply a nonlinear relationship between permittivity and glucose level in the hamster's tail (see Figure 12).
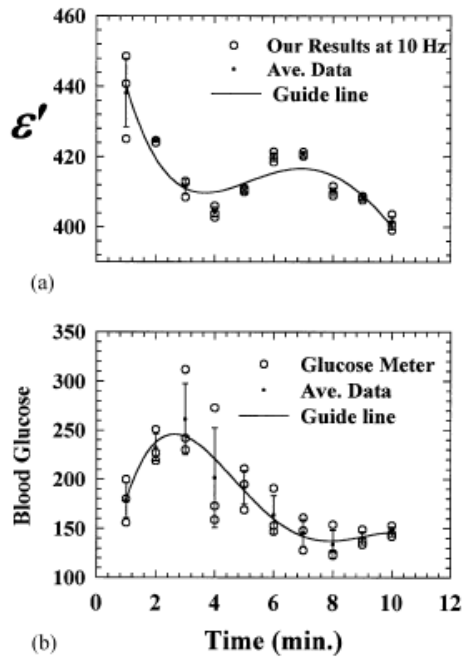
Figure 12: (a) Time dependence of ε' at 10 kHz in hamster tail and
(b) time dependence of blood glucose in hamster tail [32]

Perhaps the most encouraging and directly related research is that of Green [27].

Here, the author designed a noninvasive microwave sensor for determining blood glucose

concentration. Pulses were sent through the sensor placed on the wrist to measure the

glucose concentration. The author then drank a sugared soda while taking measurements

over the course of an hour. The results showed that the sensor was successful in

detecting permittivity changes based on glucose level.

With the knowledge of microwave properties of biological tissues and the hopeful

results of previous studies, it is possible to design a radiometer according to biomedical

specifications.

CHAPTER FOUR

Design of a Microwave Radiometer for Operation in the 4.5 to 6.5 GHz Range

Design Considerations

Operating Frequency

In designing a radiometer for biomedical purposes such as glucose monitoring, one must focus on the defining qualities of biological systems while keeping in mind the flexibility needed for future applications. The design of a biomedical radiometer is presented as a tool for laboratory use and blood glucose monitoring using the biological characteristics outlined in Chapter Three.

The design process begins with choosing an appropriate operating frequency for the radiometer. The operating frequency affects aspects such as penetration depth and spatial resolution. Microwave systems can achieve greater penetration depth than other modalities because of their lower frequencies while simultaneously distributing less energy to surrounding areas [33]. Penetration depth is defined by the equation

$$\delta = \sqrt{\frac{2}{\omega\mu\sigma}} \tag{28}$$

where ω is frequency, μ is permeability, and σ is conductivity[13]. The equation shows that penetration depth is also a function of an object's conductivity. As a wave travels through a medium, it decays at a certain rate, depending on the medium's conductivity and the frequency of the wave [13]. The higher the conductivity, the more attenuation a wave experiences during its travel, resulting in a lesser penetration depth. And, as the

frequency of the wave increases, the rate of decay also increases. For this design, a penetration depth of approximately one centimeter (cm) will suffice. The radiometer's purpose is not to detect tumors or other anomalies deep within the body, but rather to detect radiated energy closer to the skin's surface. The radiometer should utilize a location with considerable blood flow near to the surface for monitoring blood glucose concentration. Since fat contains few blood vessels, it is necessary to choose a body location that has minimal fat content, such as the underside of the wrist [27]. The penetration depth of microwaves in some biological tissues is illustrated in Figure 13 below.
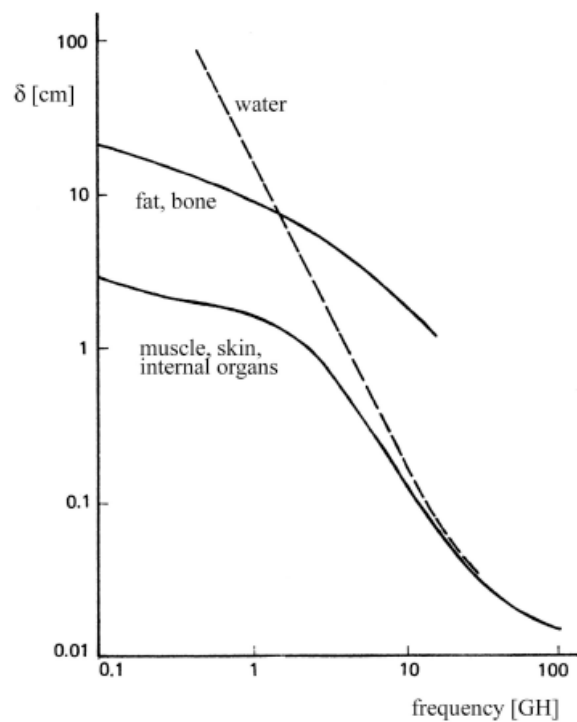
Figure 13: Penetration depth of microwaves in various tissues [2]

Another factor dependent upon operating frequency is spatial resolution. It is desirable to obtain high spatial resolution so that the radiometer can specifically "focus" on the object of measurement. Spatial resolution can be approximated by the dimensions

of the antenna aperture if the distance from the antenna to the material under test (MUT)

is in the antenna's near zone [34]. The near zone extends out to the far-field distance:

$$R_{ff} = \frac{2D^2}{\lambda} \quad [14].$$ (29)

For this study, D (the maximum antenna dimension) is 4.04 cm and λ (the antenna's

operating wavelength) is 5.21 cm. The resulting far-field distance is 6.27 cm. Therefore,

the near-field approximation is valid if the antenna aperture is within 6.27 cm of the

MUT. The approximation will most likely be applicable to this study because the

experimental procedures will involve biological materials at close range to provide the

best access to the emitted radiation.

As mentioned in Chapter 3, biological bodies are representative of their water

content, making it essential to consider the radiometer's frequency response to water.

The three important dispersion regions (β-dispersion, δ-dispersion, and γ-dispersion)

must be considered so the radiometer can detect responses due to bound and free water

relaxation. Also, referring to Figure 10, it is beneficial to choose a bandwidth that allows

the greatest discernment in permittivity among the different tissues.

A frequency range of 4.5 to 6.5 GHz was chosen for the above reasons. This

bandwidth includes frequencies low enough for sufficient penetration depth (see Figure

13) and high enough for ample spatial resolution. For an approximation, the spatial

resolution can be considered a four by two cm section on the MUT. These numbers

result from a WR159 open-ended waveguide with dimensions of 1.59 inches by 0.795

inches (or 4.04 cm by 2.02 cm). This resolution is sufficient because the radiometer is

not gathering information from one specific location (e.g. a tumor) inside the MUT, but

rather from a general area where substantial blood flow is present. The higher

frequencies of δ-dispersion as well as the lower frequencies of γ-dispersion are also included in this range (see Figures 10 and 11).

Interface

An appropriate interface must be decided upon for the boundary between the MUT and the radiometer input. The interface type depends on the nature of the MUT. An open-ended waveguide is a reasonable choice for blood glucose monitoring. With this interface, the MUT (most likely a human wrist in this case) can be placed flush against the waveguide opening so that no space exists between the MUT and the opening. This interface maximizes the signal received from the MUT with minimal interference from other sources. As a result, impedance mismatches at the tissue-air and air-antenna boundaries have been suppressed [34]. If a liquid temperature measurement is desired, a 50 Ω termination can be used as a probe to place directly into the substance. These interfaces are pictured and described in more detail in Chapter Five.

Sensitivity

Sensitivity is a significant characteristic for radiometers because it determines the minimum power difference that the radiometer can detect. Another term for sensitivity is temperature resolution, which implies the smallest temperature difference that the radiometer can decipher. Temperature changes due to any effects are minimal in biological bodies because of their inherent temperature regulatory systems. Although the precise amount of radiation emitted due to blood glucose changes is unknown, it is reasonable to assume that the amount is scarce. Also, for this study, relative moisture content differences for any application will be minute. Therefore, a high sensitivity on

the order of 0.05 Kelvin (K) is acceptable. The integration time must be flexible enough

and the noise temperature low enough to achieve the desired level of sensitivity. A

longer integration time will allow more averaging and, in effect, more smoothing of the

signal to take place. It also increases sensitivity, as evidenced by equation (21). A longer

integration time (greater than one second) can be used in this research because the

radiation levels of the MUT are not rapidly changing. And with a digital integrator, the

integration time is limited only by the microcontroller's memory capabilities.

Temperature Stability

Temperature stability is crucial to the radiometer's performance since the purpose

of the radiometer is to detect emissions of electromagnetic energy in the form of heat. A

stable temperature environment must be provided for the system if the radiometer is to

distinguish between a desired signal level of approximately -90 dBm and other sources of

emissions. This environment maintains thermal equilibrium within the system and keeps

the reference load constant. It is necessary to keep the load constant so that the antenna

signal will be compared to an identical reference temperature during each switching

cycle. Two different forms of loads exist among radiometers: a hot load and a cold load.

As their names suggest, a hot load is usually kept at room temperature or above and a

cold load is kept at a lower temperature. Many radiometers make use of liquid nitrogen

to stabilize a cold load, while heating systems and special enclosures keep hot loads

constant [35, 36]. For this design, a hot load was maintained at 40° C (313 K) by a

temperature controlling system (Watlow, St. Louis, MO). The entire radiometer system

was placed inside an insulated stainless steel box (AD Products, Cleveland, OH) to

maintain a uniform temperature. The temperature controller included a heating strip and

a thermocouple that were both mounted underneath the component panel. A temperature monitoring system (Carl's Electronics, Oakland, CA) consisting of four sensors and a microcontroller was also mounted inside the box. The sensors were placed on individual components so their temperatures could be monitored to the nearest hundredth of a degree. With this information, the radiometer output can be corrected for temperature if necessary. Figure 14 shows the radiometer system, including the temperature controlling and monitoring systems, within the enclosure. The actual enclosure for the system is pictured in Figure 15.
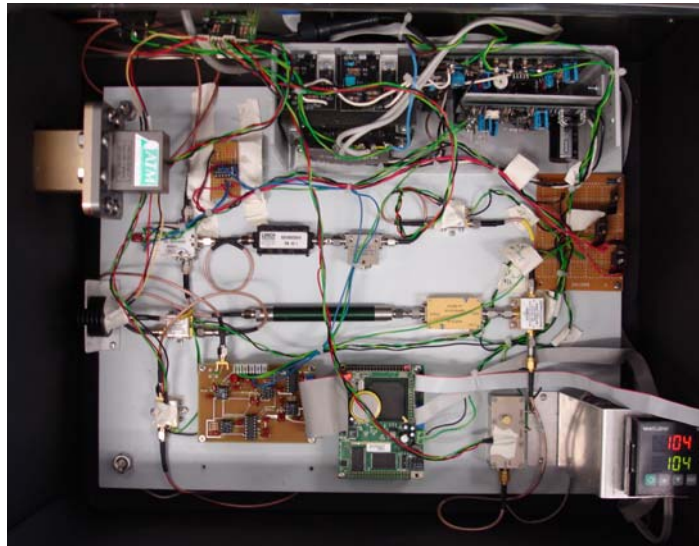
Figure 14: Photograph of system within enclosure

Figure 15: Photograph of radiometer enclosure

Configuration

As with all radiometers, it is imperative that the front end is designed with a low noise figure. A low noise front end is essential because these components have the most impact on the system's noise figure. This quantity is a measure of the reduction in the signal-to-noise ratio and is defined for a cascaded system as

$$F_{cas} = F_1 + \frac{F_2 - 1}{G_1} + \frac{F_3 - 1}{G_1 G_2} + \cdots \, , \tag{30}$$

where F_n is the noise figure and G_n is the corresponding gain of each element [14]. Insertion loss adds to the noise figure because it represents a loss in signal power that results from inserting the component into the system. The effects of gain fluctuations must also be minimized, which can be achieved by choosing the proper configuration and an appropriate switching frequency. A Dicke configuration with a superheterodyne front end and a switching frequency of 1 kHz was chosen to obtain these goals. As discussed in Chapter 2, a Dicke switch with a rapid switching frequency suppresses gain fluctuations. The superheterodyne front end adds flexibility to the instrument with band-defining filtering and frequency selectivity provided by the local oscillator (LO) frequency. An LO frequency of 4.5 GHz and a nine-section low pass filter cutoff of 600 MHz defined the IF bandwidth as DC to 600 MHz. The 600 MHz IF bandwidth presents a compromise between improving sensitivity (large bandwidth) and serving as a reasonable bandwidth for the components that follow the IF filter (small bandwidth). A block diagram of the system is displayed in Figure 16 to aid in the design discussion.
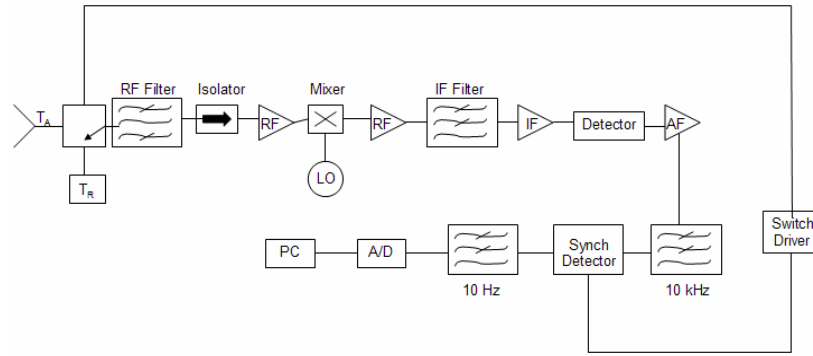
Figure 16: Block diagram of radiometer system

Specific Components

At the chosen frequency range, it is common to use coaxial components instead of waveguide components, which take up more space and are typically used in higher frequency applications. Coaxial cables and waveguides all have specific cutoff frequencies determined by their size. These frequencies establish which modes can propagate through the device. A common type of connector for coaxial cables is SubMiniature version A (SMA). SMA connectors have a frequency limit of approximately 18 GHz. All microwave components in this study, except for the horn antenna, are coaxial components with SMA connectors.

The first component after the antenna is the microwave or Dicke switch. The switch needs a low insertion loss because it is part of the low noise front end. A single-pole, double-throw (SPDT) PIN (p-type intrinsic n-type) diode switch (Custom Microwave Components, Inc., Fremont, CA) was chosen because of its 1.8 dB insertion loss and high isolation (70 dB). A switch's isolation is a measure of how well the signal is attenuated in the off position. High isolation, or attenuation, is desired so that there is no signal leakage through the off port. The switch supplies two inputs: the antenna and

the reference load. The reference load, or hot load, is a medium power microwave termination (Midwest Microwave, Saline, MI) designed for an input power rating of 10 W, with a low voltage standing wave ratio (VSWR). The power rating of the load was chosen in order to take advantage of the heat sink associated with the device. The large heat sink enables the load to reach operating temperature more quickly. The low VSWR means that most of the power is transmitted and not reflected, providing a good match between the termination and the switch. Following the switch is a bandpass filter (Lorch Microwave, Salisbury, MD) that determines the incoming signal's bandwidth. Insertion loss is more important than stop band attenuation in this segment because this filter is part of the low noise front end. Therefore, the filter was limited to five sections, resulting in an insertion loss of 0.5 dB. An isolator (Advanced Technical Materials, Patchogue, NY) was placed between the RF filter and amplifier to achieve good impedance matching and high isolation. To provide an initial boost in amplification, a low noise amplifier (Mini-Circuits, Brooklyn, NY) with a noise figure of 4.1 dB was added after the isolator. The first amplifier in the receiver chain is a key component because it essentially sets the system's noise figure. Insertion loss in the components following the first amplifier can now be disregarded because of its gain. The next component of the superheterodyne configuration is the mixer. Low conversion loss is a primary factor in choosing a mixer because it is a measure of the mixer's efficiency in converting the RF input signal to the IF output signal. Therefore, the chosen mixer (Mini-Circuits, Brooklyn, NY) has a relatively low conversion loss of 5.4 dB. The LO provides the frequency that will be mixed with the RF signal to produce the IF signal. A dielectric resonator oscillator (DRO) (Jersey Microwave, Hackettstown, NJ) with an output frequency of 4.5 GHz was

chosen for its high stability and low phase noise. The frequency drift over time is diminished with high stability. Low phase noise is a result of minimized phase fluctuations within the oscillator. When mixed with the RF signal, the LO signal produces a down-converted IF output of DC to 2 GHz, which is further amplified by another low noise amplifier (Amplical Corp., Verona, NJ). This IF amplifier adds a noise figure of 2.5 dB and a typical gain of 30 dB. To achieve the defined IF frequency, a low pass filter (Lorch Microwave, Salisbury, MD) with steep cutoffs was placed after the IF amplifier. The IF frequency range ultimately determines the radiometer bandwidth that is used for sensitivity calculations. Two cascaded amplifiers (Mini-Circuits, Brooklyn, NY) following the IF filter provide more gain to prepare the signal for detection.

As previously mentioned in Chapter 2, the output voltage of a square-law detector is proportional to the square of the input voltage, making it proportional to the input power. To operate in the square-law range, this type of detector requires an input power no higher than approximately -20 dBm [3]. A power much higher than this will take the detector out of the square-law range and into a linear range, or even further into a saturation range. The signal will become lost within the noise floor of the detector if the input power level is too low (see Figure 17 below) [14]. The input power level must be high enough to have a measurable output voltage, but low enough to maintain square-law behavior. Therefore, a level of approximately -25 dBm will be adequate. To ensure this level of power, it is necessary to calculate the signal level at the detector. Using equation (1), the radiometer input power level, assuming $T_A \approx 300$ K (close to room temperature), is -80.82 dBm. Taking into account the gains and losses of each component up to the detector, the signal level at the detector is -20.67 dBm, which is sufficiently close to the

desired signal level of -25 dBm. The Schottky diode detector (Pasternack Enterprises,

Irvine, CA) used in this study exhibits superior performance in RF circuits because of its

smaller junction capacitance in relation to other diodes.
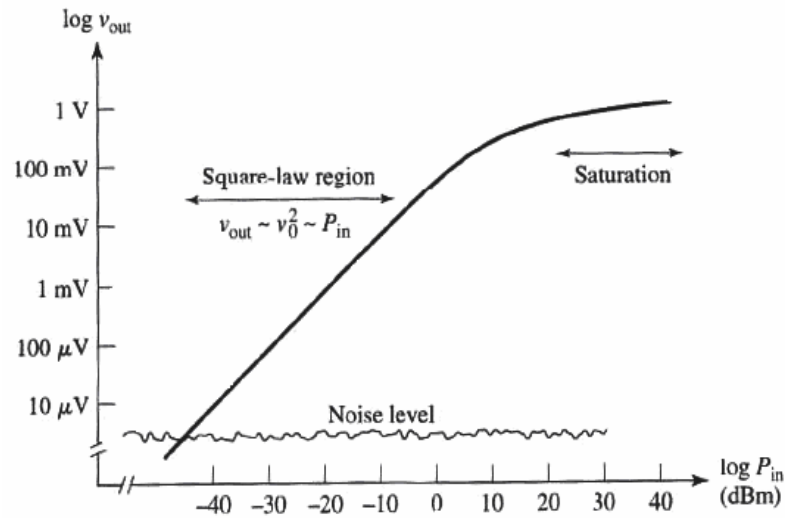
Figure 17: Square-law region for a typical diode detector [14]

Figures 18-20 below illustrate the effects of the detector on the signal. A high

frequency signal with a bandwidth of 600 MHz is enclosed in a square wave envelope

with two levels corresponding to the antenna and load positions on the switch. This is

similar to an amplitude modulated carrier signal within the envelope of the square wave

switch driver signal. The amplitude of the carrier signal changes in accordance with the

square wave's amplitude. The square wave has a frequency corresponding to the driver

frequency for the switch, which is 1 kHz in this case. The detector demodulates the

signal so that only the signal's envelope remains after detection with the same two levels

for the antenna and load. The signal is then AC coupled to remove the DC portion and

prepare the signal for the synchronous detector.
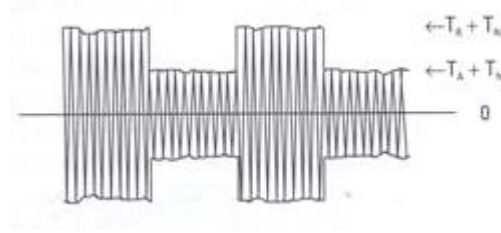
Figure 18: Signal before detection [20]
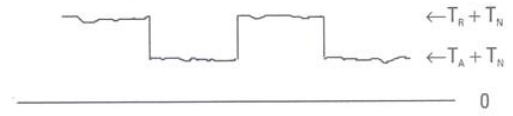
Figure 19: Signal after detection [20]
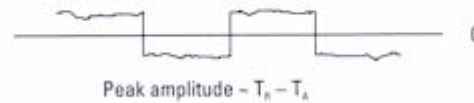
Figure 20: Signal after AC coupling [20]

The next portion of the system provides the final conditioning of the signal for the A/D converter. It includes an audio frequency (AF) amplifier with a large gain, two low pass filters, and a synchronous detector. The first filter was designed for a cutoff frequency of 10 kHz to eliminate most high frequency noise. A second low pass filter provides smoothing for the signal with a cutoff of 10 Hz. The A/D converter has an input voltage range of 0 to 5 V, meaning the signal can be significantly increased by the AF amplifier. The gain was increased simply by changing one resistor using an AD620 (Analog Devices, Norwood, MA) precision low noise instrumentation operational amplifier (op amp).

Given that the current signal is a square wave with a frequency of 1 kHz, it is beneficial to convert it to a DC signal that represents the difference between the antenna temperature and the load. A simple circuit (see Figure 21) forms the synchronous detector that performs this conversion. When the switch is open, the output is +1, while a closed switch changes the output to -1. The switch operates synchronously with the

switch driver for the microwave switch, thus multiplying the negative components by -1

and leaving the positive components unchanged. The resulting DC signal (see Figure 22)

can now be fed into the A/D converter for sampling and further integration.
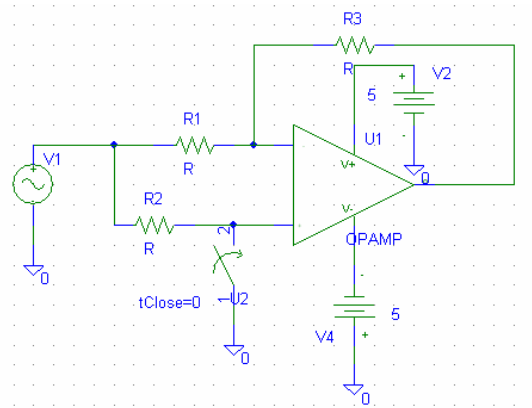
Figure 21: Synchronous detector schematic

Figure 22: Screenshots of signal (a) before and (b) after synchronous detection

The A/D converter is part of the microcontroller (Tern, Inc., Davis, CA) system

that also controls the switch driver and performs averaging on the output signal. A 16-bit

converter allows a 16-bit resolution with approximately a 76 µV voltage resolution. Two

square wave outputs were programmed at a frequency of 1 kHz for the microwave and

synchronous detector switch inputs. The A/D converter sampled the incoming DC

voltage every 500 µsec, resulting in an input sampling rate of 2 kHz. An integration time

of 10 seconds provided averages of 20,000 samples each. Since an integrator is essentially a low pass filter, the equivalent bandwidth can be found using the equation

$$B = \frac{1}{2\tau} \text{ [1]}. \tag{31}$$

Here, the low pass filter bandwidth of 0.05 Hz is well within the Nyquist sampling theorem because the sampling rate is greater than twice the bandwidth of the low pass filter. This condition eliminates aliasing, or overlap, of the reconstructed sampled signal.

A 10 second integration time is rather long compared to other integration times (5 ms to a few seconds), but it does offer the advantage of improving the radiometer's sensitivity, as presented in equation (18) [1, 3, 7, 18, 20, 36]. A longer integration time (or greater sensitivity) means that the response time of the radiometer is slower. The response time represents how quickly the radiometer can track changes in the media of interest. In this case, the integration time can be increased because the radiation being observed is not quickly changing. Another limit to integration time is the microcontroller program's memory. A 16-bit A/D converter allows 2^{16}-1, or 65,535 samples to be taken. Multiplying the number of samples by 500 μsec per sample yields approximately 32.77 seconds. This number corresponds to the maximum integration time for this radiometer. Therefore, a 10 second integration time is well within the limits.

A second function of the microcontroller system is the user interface. The interface was programmed in C programming language and provides the user with simplified access to the radiometer. The menu allows the user to choose a desired integration time, number of output readings, or default settings. Output readings are saved in a comma separated variable (csv) file and formatted into rows and columns for spreadsheet use.

The sensitivity can now be calculated using the integration time, the radiometer IF bandwidth, antenna temperature, and noise temperature. The noise figures and insertion losses of each component up to and including the RF amplifier are:

PIN diode switch: 1.80 dB
RF filter: 0.50 dB
Isolator: 0.35 dB
RF amplifier: 4.10 dB
Total noise figure: 6.75 dB.

The total noise figure is represented by F1 in equation (30) and the other terms can be neglected because of the significant gain on the first amplifier. The noise figure is converted from dB to 4.73 and is substituted into the noise temperature equation:

$$T_N = T_0(\text{NF-1}). \tag{32}$$

Using $T_0 \approx 290$ K (a universally defined value), the equation produces a noise temperature of 1082 K [1]. Equation (18) can now be used to calculate the radiometer's sensitivity. Assuming $T_A \approx 300$ K and using the IF bandwidth (600 MHz) for B gives a sensitivity of 0.036 K, which is within range of the desired specifications.

The designed radiometer now fits is biomedical specifications. Its experimental results for biomedical tests are outlined in the following chapter.

CHAPTER FIVE

Experimental Results

Three separate experiments were performed with the radiometer. One experiment

verified the sensor performance and demonstrated the repeatability and sensitivity of the

device. The other two experiments illustrated the performance of the radiometer as a

biomedical sensor.

Experiment One

Materials and Methods

This experiment's focus was to verify the radiometer's repeatability and

sensitivity. The results of this experiment are used to produce a calibration curve to serve

as a basis for future experiments. The radiometer's performance can be validated before

every experiment by referencing these results. This validation experiment must measure

known parameter values that can be easily reproduced. A simple test using different

temperatures of water was designed for this reason. Each water validation experiment

uses up to seven different temperatures ranging from 0° C to 100° C. The two

temperature extremes, freezing and boiling, represent known values that can be repeated

during each experiment. An ice bath was used for freezing water and a Corning

Scholar^{TM} 170 hot plate (Corning, Inc., Acton, MA) provided boiling water in a metal

canister. Other temperatures were obtained using a coffee mug placed on a candle

warmer (Provo Craft and Novelty, Spanish Fork, UT), a Pyrex® (Corning, Inc., Acton,

MA) beaker placed on the hot plate, a plastic bowl filled with room temperature water, and an insulated thermos filled with cool water. The 50 Ω termination (S.M. Electronics, Fairview, TX) mentioned in Chapter Four was used as a probe to place directly into the containers of water. The termination is a resistive load that allows the radiometer to effectively measure the physical temperature of the water using the principles discussed in Chapter Two. The termination and approximately three inches of the connected cable were dipped in a rubber coating four times (Plasti Dip, Blaine, MN) to prevent water from leaking inside the connection. The radiometer input was configured so that the termination cable could be directly connected to an input on the microwave switch. For this arrangement, the antenna was disconnected from the bulkhead feed-through (the interface between the antenna and the microwave switch) (Precision Waveguide, Hernando, FL) and insulation was inserted into the feed-through to maintain thermal equilibrium inside the box (see Figure 23 below).
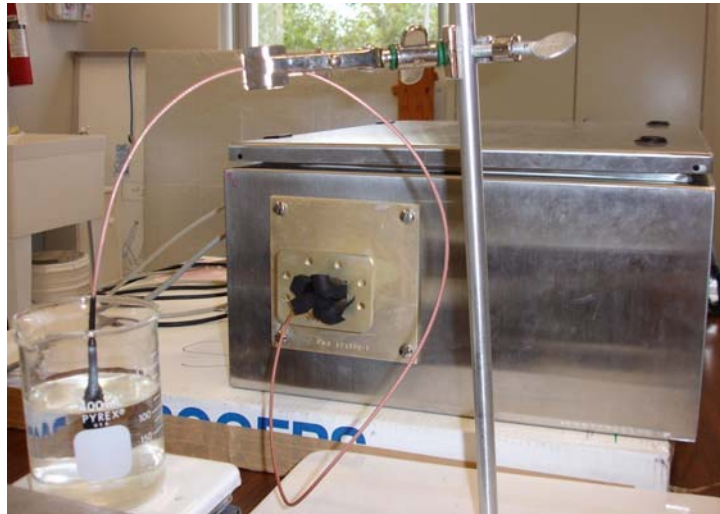
Figure 23: Picture of experimental setup for water validation experiments

A clamp prevented the termination from touching any part of the containers so only the water temperature, and not the container temperature, was measured. A K-type thermocouple calibrator with 0.007% accuracy and 0.1° resolution (Altek, Rochester, NY) was placed directly into the water while taking measurements. The radiometer was configured for a ten second integration time and ten readings per sample, with each reading representing 20,000 A/D samples. The termination was given approximately ten minutes to stabilize within each different water temperature. After the measurement was complete, the termination was placed into a different water container chosen at random.

Results

Nine separate experiments were performed over the course of three weeks with at least thirty minutes between each experiment. All experiments were combined to produce a single calibration curve. The ten readings for each temperature sample in each experiment were averaged together to provide one data point per sample. The radiometer output voltage from the A/D converter was then plotted against thermocouple temperature for each individual sample. Figure 24 below illustrates the data fit to a second-order polynomial trend line with an R-squared (or coefficient of determination) value of 0.9953.

The square root of the voltage was applied to each data point to transform the data into a linear relationship representing radiometer temperature versus thermocouple temperature. This transformation produces a calibration curve and equation that can be used as a foundation for future experiments. Figure 25 presents the radiometer calibration curve resulting from the combined water validation experiments. The calibration equation is

$$T = \frac{\sqrt{V} - 0.1281}{0.0042}, \tag{33}$$

where T is the temperature in degrees Celsius and V is the radiometer output voltage in volts.

Combined Water Validation Experiments
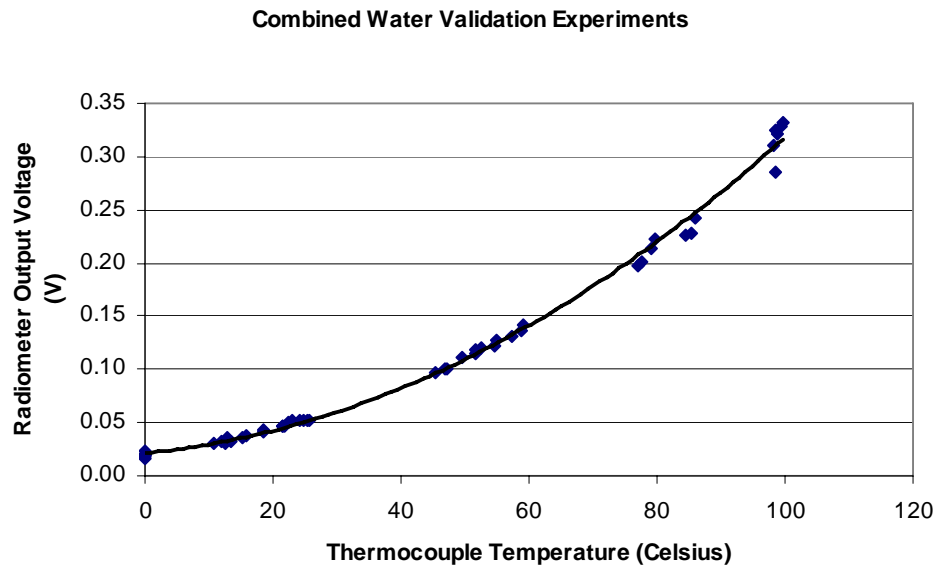
Figure 24: Results from combined water validation experiments

Combined Water Validation Experiments
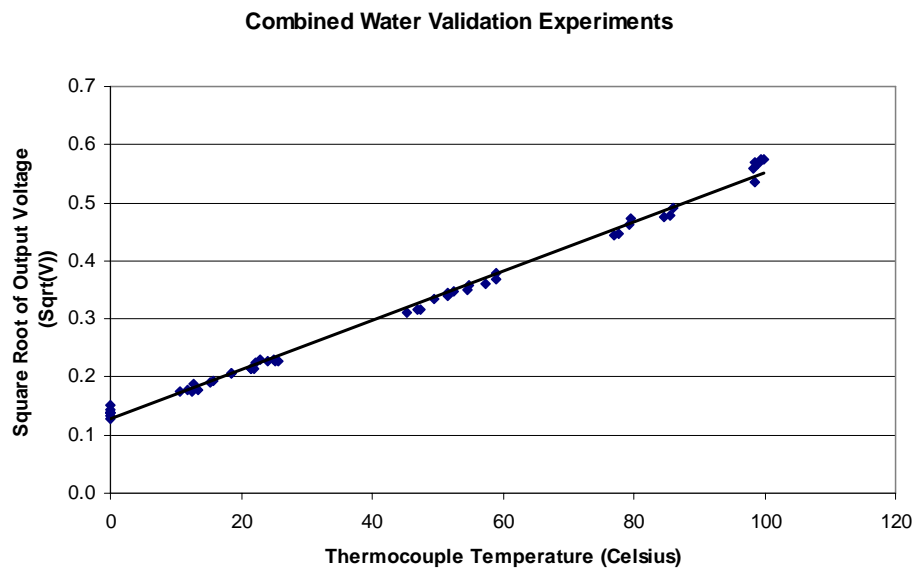
Figure 25: Radiometer calibration curve

Discussion

The results demonstrate that the radiometer is exhibiting repeatable behavior. The coefficient of determination, R-squared, is 0.9947 for the combined water validation experiments. The statistical analysis was performed using SAS (SAS Institute, Inc., Cary, NC) and is documented in Appendix A.

Experiment Two

Methods and Materials

The next experiment illustrates the radiometer's performance as a biomedical sensor. As discussed in Chapter Three, biological materials are comprised mostly of water and exhibit properties directly related to water content. This experiment tests the radiometer's ability to discern among varying water contents placed into a heterogeneous substance. Nine vials were labeled with numbers and weighed using an analytical balance with a precision of 0.01 milligrams (Mettler-Toledo, Columbus, OH). Equal amounts of cornmeal were then added to each vial. All vials were placed in an oven at 55°C to remove any existing antecedent moisture content of the cornmeal. A low baking temperature and periodic weighing prevented over drying the cornmeal so that any bound water was not removed. If the bound water is removed, the molecular properties of the cornmeal change, which causes further alterations in the cornmeal's electrical properties. The mass of each vial was checked after one hour and again after one hour and forty-five minutes. After verifying a constant mass, the vials were removed from the oven and immediately sealed. Each mass was measured again before any water was added. Precise amounts of water ranging from no water to 600 microliters (μL) were added to

each vial using pipettes (see Figure 26). The vials were then sealed again and weighed

(see Figure 27).

Figure 26: Adding water to cornmeal using pipette
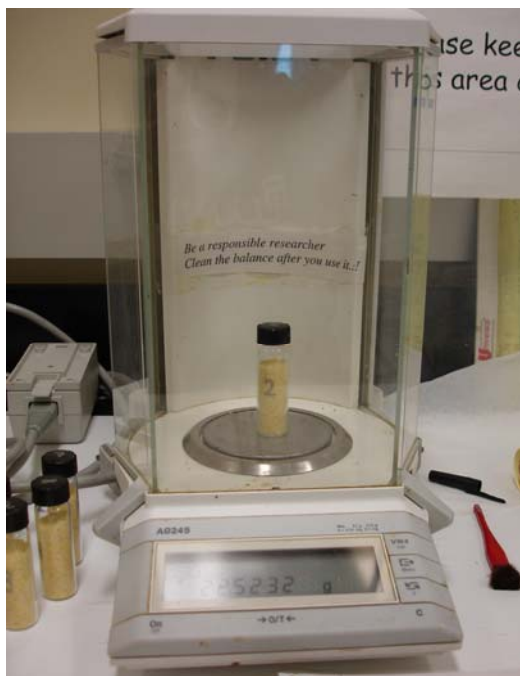
Figure 27: Vial with cornmeal and water weighed with analytical balance

The vials were stored safely in a refrigerator for two days so the water would have ample

time to soak into the cornmeal. After removing the vials from the refrigerator, they were

weighed again and were then ready for use. The table below outlines the mass of each

vial at different stages during the preparation process (all units in grams).

Table 1: Mass of each vial at different stages of preparation

Vial	Empty Vial	Cornmeal	Vial with Cornmeal	Vial with Cornmeal After Drying	Vial with Cornmeal and Water	Water	Vial After Two Days in Refrigerator
1	14.4018	8.0100	22.4118	22.3157	22.3157	0.0000	22.3179
2	14.5807	8.0147	22.5947	22.5019	22.5222	0.0203	22.5233
3	14.5337	8.0508	22.5845	22.4907	22.5415	0.0508	22.5424
4	14.4971	7.8972	22.3943	22.3039	22.3546	0.0507	22.3556
5	14.6331	7.8870	22.5201	22.4279	22.7270	0.2991	22.7281
6	14.6079	7.9945	22.6024	22.5193	22.8191	0.2998	22.8206
7	14.5627	7.9948	22.5575	22.4724	22.7814	0.3090	22.7826
8	14.5528	8.0694	22.6222	22.5367	22.9323	0.3956	22.9323
9	14.6432	7.9447	22.5879	22.5003	23.0935	0.5932	23.0952

The radiometer setup utilized a straight section of WR159 waveguide (Precision

Waveguide, Hernando, FL) connected to the bulkhead feed through with the other end

terminated with a shorting plate. A hole was cut a quarter wavelength from the far end of

the waveguide for the vial. As a result, the location of the vial represented an open

circuit and any signals radiated away from the system would reflect back toward the

radiometer input.

Referring to Chapter Two, non-homogeneous surfaces contribute to variations in

emissivity, which causes fluctuations in the radiometer output. Cornmeal emits radiation

in many different directions depending upon its geometry because of its non-

homogeneity. The vial's position inside the waveguide will also have an effect on the

emitted radiation. Therefore, it is necessary to eliminate these fluctuations so the

radiometer output will exhibit more consistent behavior. A turntable was used to spin the vial as measurements were taken throughout the spin cycles. Spinning the vial allows averaging of the geometrical variations so their effects are not as prominent. The turntable was programmed to spin two revolutions in 200 seconds. An integration time of ten seconds with twenty readings was programmed for each cornmeal sample. Vials were then placed in random order into the waveguide (see Figure 28). Temperature data was taken with the monitoring system inside the radiometer so the data could be corrected for temperature.
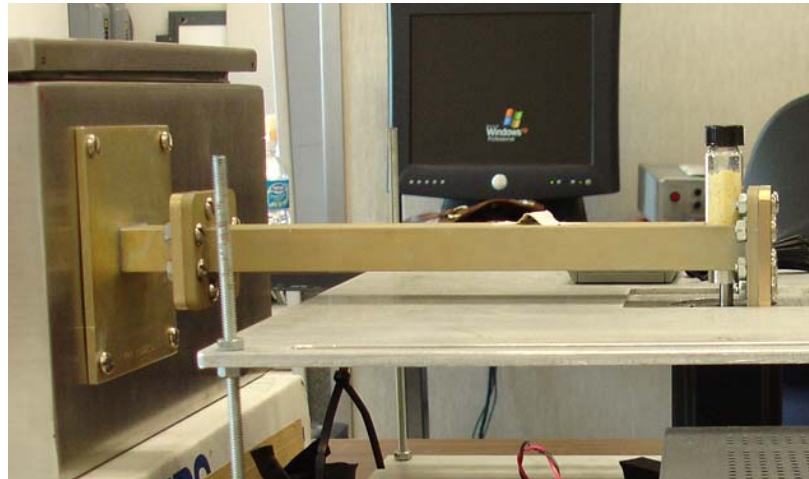
Figure 28: Setup for cornmeal experiments

Results

Three separate cornmeal experiments were performed with approximately thirty minutes between each experiment. The twenty readings for each sample were averaged to produce one voltage data point. The data was then temperature corrected for variations in the reference load temperature. From equation (20), the output voltage of a Dicke radiometer depends on the reference temperature. The average of the reference load temperatures, T, for each sample was divided by 40 (the desired reference temperature,

T_R) to obtain the ratio T/T_R, which is denoted as Θ. This value provides a number that can be used with each data point to eliminate the temperature dependence of the output voltage upon the reference load temperature. Figure 29 below illustrates the output voltage versus water content for the three combined experiments.

Combined Cornmeal Data (Temperature Corrected)
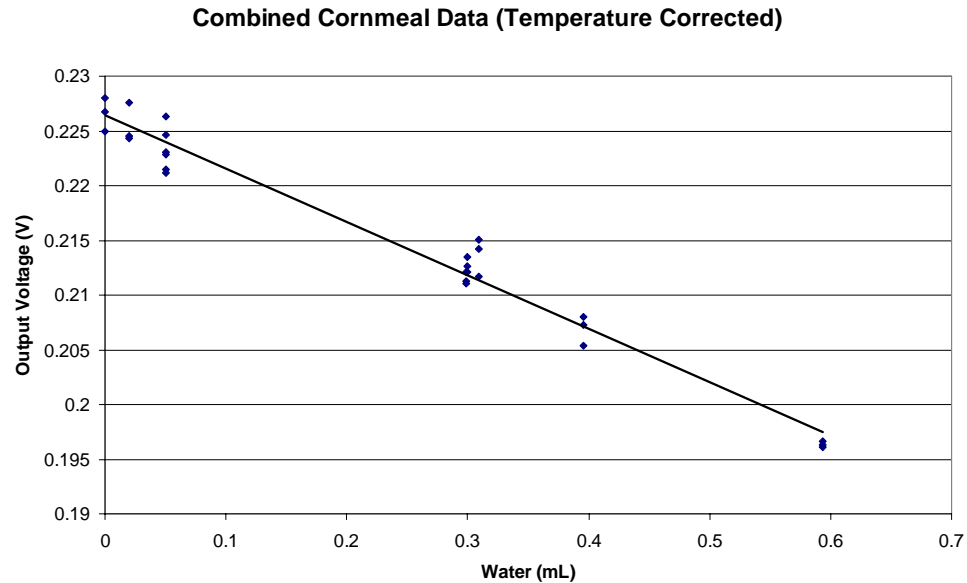
Figure 29: Results from combined cornmeal experiments

Using a repeated measures analysis, the type 3 tests of fixed effects did not show a significant difference from one experiment to the next (See Appendix B). The R-squared for the temperature corrected cornmeal data is 0.9725.

Discussion

The results noticeably demonstrate water's effect on the cornmeal's emitted radiation. Chapter Three explained how water content relates to permittivity and emissivity. Higher water content leads to greater permittivity (see Figure 10) and lower emissivity, resulting in a lower radiometer output voltage. This phenomenon is evident

by the negative slope in output voltage as water content increases. Comparing Figure 29

to Figure 25, more scatter is apparent in the cornmeal experiments. Also, less scatter

occurs as water content increases in Figure 29. These effects could be due to water

absorption by the top layers of the cornmeal. It is possible that the water did not descend

toward the bottom of the vial after it was deposited. For the most accurate

measurements, the water must reside within the bottom section of the vial that was placed

directly into the waveguide (see Figure 28). Otherwise, the radiometer input cannot

detect a significant amount of radiation due to water content. The scattering effects can

be further explained using the geometric principles mentioned in Chapter Two and earlier

in this chapter. Greater water content packs the cornmeal together, causing more

homogeneity within the medium. Minimizing geometric diversity produces more precise

measurements, as evidenced by the diminished scatter with increasing water content.

Also, vial placement in the waveguide and non-uniform vial thickness increase geometric

variability in the results.

Experiment Three

Materials and Methods

The final experiment demonstrates the radiometer's performance as a blood

glucose sensor. The experiment tests the radiometer's ability to detect radiation using a

sugared soda [27]. The user fasted for twelve hours before taking measurements. The

radiometer was configured with an open-ended waveguide bulkhead feed through so the

wrist could be placed flush against the opening. The wrist was taped to the opening to

reduce any movement that might have caused discrepancies due to geometric variations

within the arm (see Figures 30-31). Before the user quickly drank a sugared soda,

radiometric measurements were taken for thirty minutes. The radiometer was configured

with a ten second integration time and ten readings per time sample. Data was recorded

for one hour after drinking the soda.

Figure 30: Overhead view of blood
glucose experimental setup

Figure 31: Side view of blood glucose experimental setup

Results

Data was taken every three minutes over a total period of ninety minutes. The

output voltages were then plotted against time, as illustrated in Figure 32. A two-point

moving average was then fitted to the data to highlight the voltage trends. The distance

between each data point represents a time lapse of three minutes. The time before

drinking the soda spans from 0 to 1440 seconds.
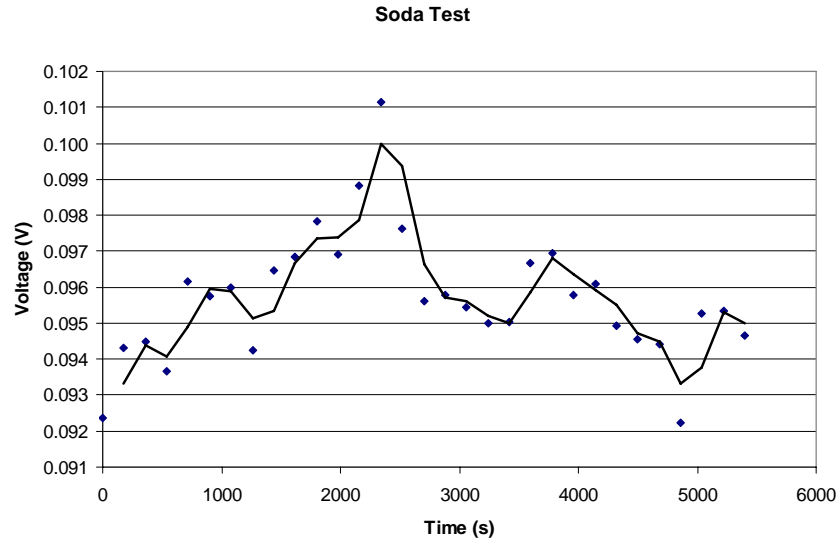
Soda Test

Figure 32: Results from soda test processed with 2-point moving average

Discussion

The results indicate a clear increase in voltage after drinking the soda. A sharp

decrease follows, indicating insulin secretion, the hormone responsible for regulating

glucose levels. The graph was expected to reveal a relatively constant trend for the time

prior to drinking the soda. The varying voltage trend is explained by the cephalic

phenomenon, which states that simply smelling, seeing, or thinking of food can trigger

premature insulin secretion [37]. During this phase, the body prepares the stomach for

the ingestion of food and initiates the body's natural glucose regulatory system [27, 37].

The post-consumption region is indicative of the radiometer's reaction to glucose.

Referring to Figure 12 and the principles discussed in Chapter Three, as glucose

increases, permittivity decreases, resulting in an increase in emissivity and, in effect,

output voltage. The results demonstrate the voltage response due to the body's emitted

radiation and permittivity changes after consumption of the soda.

CHAPTER SIX

Conclusions and Final Recommendations

The design and implementation of a microwave radiometer for biomedical applications was presented in this study. Experimental results validated the radiometer's repeatability and performance as a biomedical sensor. A definite correlation between water temperature and radiometer brightness temperature was revealed with the water validation experiments. The results from the cornmeal experiments presented a relationship between water content and radiometer brightness temperature. The radiometer also exhibited positive results for the monitoring of naturally emitted electromagnetic radiation due to glucose level changes.

Further research on the microwave properties of biological substances would aid in the development of this radiometer. Human bodies present many variables, such as blood volume, skin depth, water content, and body fat percentage [27]. These variables add complicated dimensions that may or may not affect the radiometer's ability to perform accurate biological assessments. More specifically, information needs to be gathered about the effects of biological processes on radiation emission. Although the results from the blood glucose test seemingly followed a trend between glucose and radiation emission, a thorough understanding of the biological causes of radiation emission must be obtained.

Some modifications can be made to the system to further enhance its performance and functionality. For example, adding a small fan inside the radiometer box would aid in air circulation while the temperature control system is running. The fan would allow the box to rise to a more uniform temperature at a faster rate. It would also be advantageous to use shielded wires for the power cord and data lines. This type of wiring would minimize system noise due to conducted RF interference.

The current radiometer demonstrates the ability to monitor physiological responses due to glucose changes both passively and non-invasively. Although this radiometer is an encouraging beginning, it still requires adjustments before it is of practical use for glucose monitoring. The system's bulk poses a limit on how and where it can be used. It may be that a radiometer can be placed in a doctor's office or grocery store for blood glucose monitoring, similar to the current blood pressure monitors. Also, further calibration is necessary for the radiometer to deliver a single number representing glucose concentration.

The presented radiometer is a positive step toward discovering noninvasive and passive methods for biomedical diagnostics. This study outlined the birth of a device that can continue its laboratory use for many future experiments. Its safe operation provides an alternative to current biomedical measurement techniques.

APPENDICES

APPENDIX A

Statistical Analysis for Water Validation Experiments

Calibration Curve and SAS Report for Voltage vs. Thermocouple Temperature

All Calibration Curves Combined
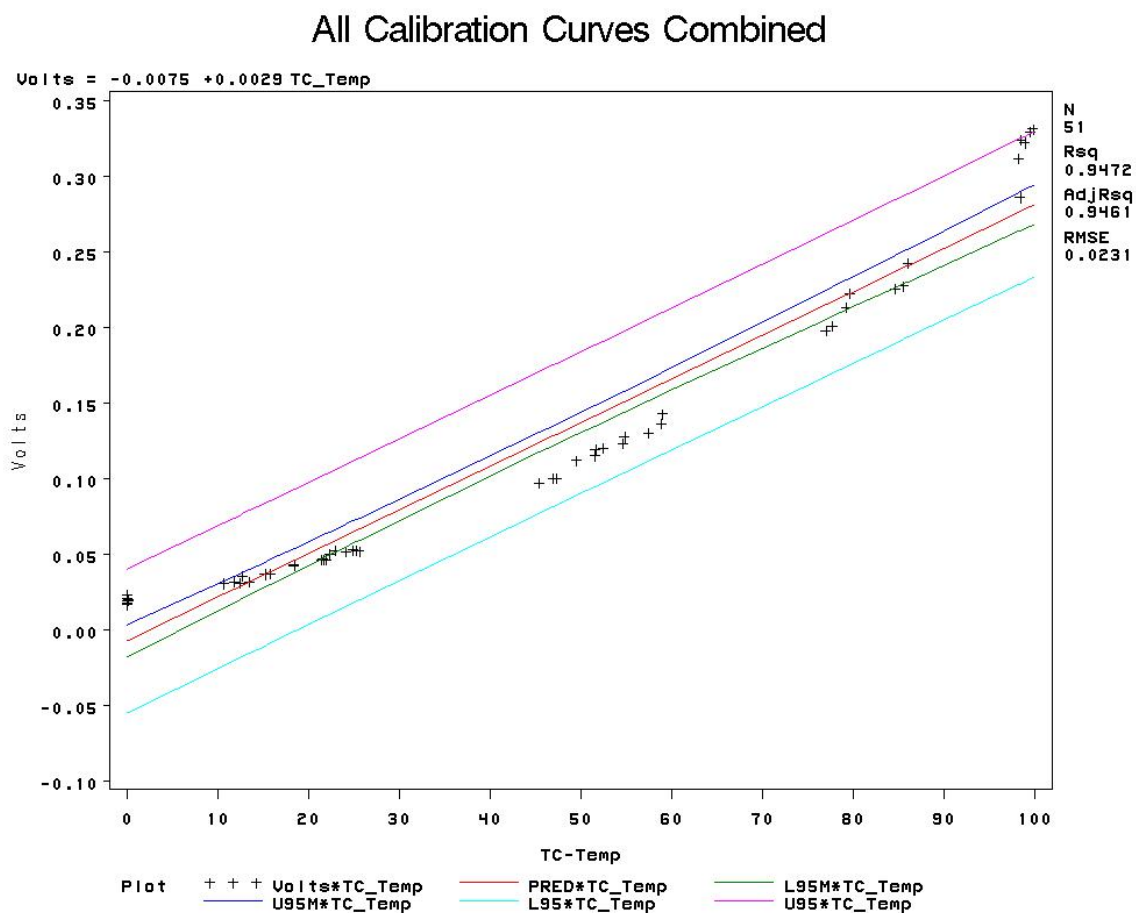
Figure A.1: Calibration curve for output voltage vs. thermocouple temperature showing nonlinearity

```
                                test dump                    13:56 Thursday, October 5, 2006

          Obs    Expt     TC_Temp      Volts      SR_Volts

            1      1         0.1       0.01945     0.13945
            2      1        15.8       0.03699     0.19232
            3      1        21.6       0.04642     0.21545
            4      1        47.3       0.10022     0.31658
            5      1        59.0       0.14266     0.37770
            6      1        77.7       0.20063     0.44791
            7      1        84.6       0.22541     0.47477
            8      2         0.0       0.01936     0.13913
            9      2        18.4       0.04263     0.20648
           10      2        21.9       0.04629     0.21515
           11      2        45.4       0.09678     0.31110
           12      2        57.4       0.13016     0.36078
           13      2        79.2       0.21308     0.46160
```

```
          14      2      86.0      0.24231      0.49225
          15      3      11.8      0.03165      0.17790
          16      3      21.4      0.04625      0.21506
          17      3      46.9      0.09997      0.31618
          18      3      58.9      0.13639      0.36931
          19      3      77.0      0.19766      0.44459
          20      3      85.5      0.22728      0.47673
          21      4      22.3      0.04989      0.22336
          22      4      49.5      0.11181      0.33438
          23      4       0.1      0.01928      0.13885
          24      4      98.9      0.32213      0.56756
          25      4      12.7      0.03523      0.18770
          26      5      79.6      0.22252      0.47172
          27      5      22.9      0.05237      0.22884
          28      5       0.0      0.02313      0.15207
          29      5      99.8      0.33117      0.57547
          30      5      15.2      0.03655      0.19117
          31      5      54.8      0.12738      0.35691
          32      6      25.3      0.05207      0.22819
          33      6      52.4      0.12006      0.34649
          34      6       0.0      0.01779      0.13339
          35      6      12.4      0.03060      0.17493
          36      6      98.4      0.32422      0.56940
          37      7      24.9      0.05257      0.22927
```

                                    test dump   13:56 Thursday, October 5, 2006

```
          Obs    Expt    TC_Temp    Volts     SR_Volts

          38      7      18.4      0.04212      0.20522
          39      7       0.0      0.01892      0.13755
          40      7      54.6      0.12291      0.35059
          41      7      98.4      0.28595      0.53475
          42      8      25.6      0.05186      0.22772
          43      8      51.5      0.11509      0.33925
          44      8      98.2      0.31140      0.55803
          45      8       0.0      0.01650      0.12843
          46      8      13.5      0.03170      0.17805
          47      9      24.1      0.05151      0.22697
          48      9       0.0      0.02027      0.14238
          49      9      99.5      0.32928      0.57383
          50      9      51.6      0.11902      0.34499
          51      9      10.7      0.03036      0.17424
```

                              All Calibration Curves Combined   13:56 Thursday, October 5, 2006

                                    The REG Procedure
                                    Model: MODEL1
                              Dependent Variable: Volts Volts

                                    Analysis of Variance

Source	DF	Sum of Squares	Mean Square	F Value	Pr > F
Model	1	0.46845	0.46845	879.23	<.0001
Error	49	0.02611	0.00053280		
Corrected Total	50	0.49456			

Root MSE	0.02308	R-Square	0.9472
Dependent Mean	0.11328	Adj R-Sq	0.9461
Coeff Var	20.37671		

                                    Parameter Estimates

Variable	Label	DF	Parameter Estimate	Standard Error	t Value	Pr > |t|
Intercept	Intercept	1	-0.00748	0.00520	-1.44	0.1567
TC_Temp	TC-Temp	1	0.00289	0.00009746	29.65	<.0001

                              All Calibration Curves Combined   13:56 Thursday, October 5, 2006

                                    The REG Procedure
                                    Model: MODEL1
                              Dependent Variable: Volts Volts

                                    Output Statistics

Obs	Dep Var Volts	Predicted Value	Std Error Mean Predict	95% CL Mean		95% CL Predict		Residual	Std Error Residual	Student Residual	-2-1 0 1 2
1	0.0194	-0.007190	0.005192	-0.0176	0.003243	-0.0547	0.0404	0.0266	0.0225	1.184	| **
2	0.0370	0.0382	0.004106	0.0299	0.0464	-0.008935	0.0853	-0.001192	0.0227	-0.0525	|
3	0.0464	0.0549	0.003784	0.0473	0.0625	0.007935	0.1019	-0.008522	0.0228	-0.374	|
4	0.1002	0.1292	0.003277	0.1226	0.1358	0.0824	0.1761	-0.0290	0.0228	-1.269	** |
5	0.1427	0.1630	0.003642	0.1557	0.1703	0.1161	0.2100	-0.0204	0.0228	-0.893	* |
6	0.2006	0.2171	0.004764	0.2075	0.2266	0.1697	0.2644	-0.0164	0.0226	-0.727	* |
7	0.2254	0.2370	0.005278	0.2264	0.2476	0.1894	0.2846	-0.0116	0.0225	-0.516	* |
8	0.0194	-0.007479	0.005199	-0.0179	0.002970	-0.0550	0.0401	0.0268	0.0225	1.193	| **
9	0.0426	0.0457	0.003955	0.0377	0.0536	-0.001369	0.0928	-0.003059	0.0227	-0.135	|
10	0.0463	0.0558	0.003769	0.0482	0.0634	0.008807	0.1028	-0.009519	0.0228	-0.418	|
11	0.0968	0.1237	0.003251	0.1172	0.1302	0.0769	0.1706	-0.0269	0.0229	-1.179	** |
12	0.1302	0.1584	0.003572	0.1512	0.1656	0.1115	0.2053	-0.0282	0.0228	-1.238	** |
13	0.2131	0.2214	0.004872	0.2116	0.2312	0.1740	0.2688	-0.008312	0.0226	-0.368	|
14	0.2423	0.2410	0.005386	0.2302	0.2519	0.1934	0.2887	0.001267	0.0224	0.0564	|
15	0.0316	0.0266	0.004358	0.0179	0.0354	-0.0206	0.0738	0.005027	0.0227	0.222	|
16	0.0463	0.0544	0.003794	0.0467	0.0620	0.007354	0.1014	-0.008112	0.0228	-0.356	|
17	0.1000	0.1281	0.003270	0.1215	0.1346	0.0812	0.1749	-0.0281	0.0228	-1.229	** |
18	0.1364	0.1627	0.003637	0.1554	0.1700	0.1158	0.2097	-0.0263	0.0228	-1.155	** |
19	0.1977	0.2150	0.004714	0.2056	0.2245	0.1677	0.2624	-0.0174	0.0226	-0.769	* |
20	0.2273	0.2396	0.005347	0.2288	0.2503	0.1920	0.2872	-0.0123	0.0225	-0.549	* |

```
21  0.0499   0.0570  0.003749   0.0494  0.0645  0.009969   0.1040 -0.007073  0.0228  -0.311  |       |
22  0.1118   0.1356  0.003318   0.1289  0.1422  0.0887     0.1824  -0.0238   0.0228  -1.040  | **    |
23  0.0193 -0.007190 0.005192  -0.0176 0.003243 -0.0547    0.0404   0.0265   0.0225   1.177  |       | **
24  0.3221   0.2783  0.006436   0.2654  0.2913  0.2302     0.3265   0.0438   0.0222   1.976  |       | ***
25  0.0352   0.0292  0.004299   0.0206  0.0379 -0.0180     0.0764  0.006012  0.0227   0.265  |       |
26  0.2225   0.2225  0.004902   0.2127  0.2324  0.1751     0.2700 -0.000022  0.0226  -0.0010 |       |
27  0.0524   0.0587  0.003720   0.0512  0.0662  0.0117     0.1057 -0.006327  0.0228  -0.278  |       |
28  0.0231 -0.007479 0.005199  -0.0179 0.002970 -0.0550    0.0401   0.0306   0.0225   1.361  |       | **
29  0.3312   0.2809  0.006512   0.2678  0.2940  0.2327     0.3291   0.0502   0.0221   2.269  |       | ****
30  0.0365   0.0364  0.004143   0.0281  0.0448 -0.0107     0.0836 0.0000998  0.0227   0.00440 |      |
```

All Calibration Curves Combined   13:56 Thursday, October 5, 2006

The REG Procedure
Model: MODEL1
Dependent Variable: Volts Volts

Output Statistics

| | Cook's |
Obs	D
1	0.037
2	0.000
3	0.002
4	0.017
5	0.010
6	0.012
7	0.007
8	0.038
9	0.000
10	0.002
11	0.014
12	0.019
13	0.003
14	0.000
15	0.001
16	0.002
17	0.015
18	0.017
19	0.013
20	0.009
21	0.001
22	0.011
23	0.037
24	0.165
25	0.001
26	0.000
27	0.001
28	0.049
29	0.223
30	0.000

All Calibration Curves Combined   13:56 Thursday, October 5, 2006

The REG Procedure
Model: MODEL1
Dependent Variable: Volts Volts

Output Statistics

```
     Dep Var Predicted   Std Error                                    Std Error  Student
Obs   Volts    Value   Mean Predict    95% CL Mean      95% CL Predict     Residual  Residual  Residual  -2-1 0 1 2

31  0.1274   0.1509  0.003472   0.1439  0.1579  0.1040  0.1978  -0.0235  0.0228  -1.030  | **    |
32  0.0521   0.0656  0.003610   0.0584  0.0729  0.0187  0.1126  -0.0136  0.0228  -0.595  |  *    |
33  0.1201   0.1439  0.003394   0.1371  0.1508  0.0971  0.1908  -0.0239  0.0228  -1.046  | **    |
34  0.0178 -0.007479 0.005199  -0.0179 0.002970 -0.0550 0.0401   0.0253  0.0225   1.124  |       | **
35  0.0306   0.0284  0.004319   0.0197  0.0370 -0.0188  0.0755  0.002248 0.0227   0.0991 |       |
36  0.3242   0.2769  0.006394   0.2640  0.2897  0.2287  0.3250   0.0473  0.0222   2.135  |       | ****
37  0.0526   0.0645  0.003627   0.0572  0.0718  0.0175  0.1114  -0.0119  0.0228  -0.522  |  *    |
38  0.0421   0.0457  0.003955   0.0377  0.0536 -0.001369 0.0928 -0.003578 0.0227  -0.157  |       |
39  0.0189 -0.007479 0.005199  -0.0179 0.002970 -0.0550 0.0401   0.0264  0.0225   1.174  |       | **
40  0.1229   0.1503  0.003465   0.1433  0.1573  0.1034  0.1972  -0.0274  0.0228  -1.200  | **    |
41  0.2860   0.2769  0.006394   0.2640  0.2897  0.2287  0.3250  0.009082 0.0222   0.410  |       |
42  0.0519   0.0665  0.003597   0.0593  0.0737  0.0196  0.1134  -0.0146  0.0228  -0.642  |  *    |
43  0.1151   0.1413  0.003368   0.1346  0.1481  0.0945  0.1882  -0.0263  0.0228  -1.150  | **    |
44  0.3114   0.2763  0.006377   0.2635  0.2891  0.2282  0.3244   0.0351  0.0222   1.582  |       | ***
45  0.0165 -0.007479 0.005199  -0.0179 0.002970 -0.0550 0.0401   0.0240  0.0225   1.066  |       | **
46  0.0317   0.0315  0.004248   0.0230  0.0401 -0.0156  0.0787  0.000168 0.0227   0.00740 |      |
47  0.0515   0.0622  0.003663   0.0548  0.0695  0.0152  0.1091  -0.0106  0.0228  -0.467  |       |
48  0.0203 -0.007479 0.005199  -0.0179 0.002970 -0.0550 0.0401   0.0278  0.0225   1.234  |       | **
49  0.3293   0.2801  0.006487   0.2670  0.2931  0.2319  0.3282   0.0492  0.0222   2.222  |       | ****
50  0.1190   0.1416  0.003371   0.1349  0.1484  0.0948  0.1885  -0.0226  0.0228  -0.990  |  *    |
51  0.0304   0.0234  0.004430   0.0145  0.0323 -0.0238  0.0707  0.006916 0.0227   0.305  |       |
```

Output Statistics

| | Cook's |
Obs	D
31	0.012
32	0.004
33	0.012

All Calibration Curves Combined   13:56 Thursday, October 5, 2006

The REG Procedure
Model: MODEL1
Dependent Variable: Volts Volts

Output Statistics

```
                                   Cook's
                      Obs             D

                       34          0.034
                       35          0.000
                       36          0.189
                       37          0.003
                       38          0.000
                       39          0.037
                       40          0.017
                       41          0.007
                       42          0.005
                       43          0.014
                       44          0.103
                       45          0.030
                       46          0.000
                       47          0.003
                       48          0.041
                       49          0.212
                       50          0.011
                       51          0.002


             Sum of Residuals                        0
             Sum of Squared Residuals           0.02611
             Predicted Residual SS (PRESS)      0.02909
```

Calibration Curve and SAS Report for Transformed Voltage
vs. Thermocouple Temperature
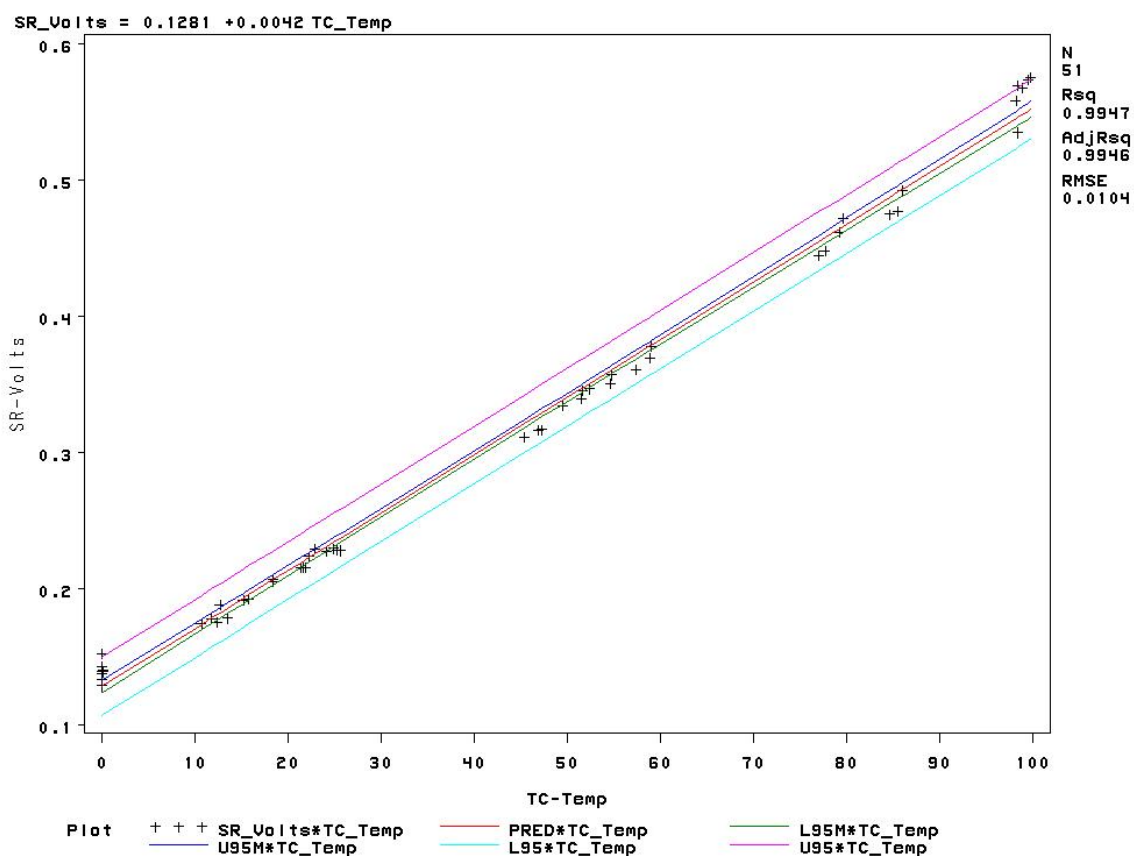
Figure A.2: Calibration curve for square root of output voltage vs. thermocouple temperature

```
                              The REG Procedure
                               Model: MODEL2
                     Dependent Variable: SR_Volts SR-Volts

                            Analysis of Variance

                                   Sum of          Mean
     Source              DF       Squares        Square    F Value    Pr > F

     Model                1       1.01102       1.01102    9283.68    <.0001
     Error               49       0.00534    0.00010890
     Corrected Total     50       1.01636


                Root MSE              0.01044    R-Square    0.9947
                Dependent Mean        0.30553    Adj R-Sq    0.9946
                Coeff Var             3.41557


                            Parameter Estimates

                                    Parameter      Standard
     Variable    Label        DF     Estimate         Error    t Value    Pr > |t|

     Intercept   Intercept     1      0.12813       0.00235      54.51     <.0001
     TC_Temp     TC-Temp       1      0.00425    0.00004406      96.35     <.0001


                 All Calibration Curves Combined      13:56 Thursday, October 5, 2006

                              The REG Procedure
                               Model: MODEL2
                     Dependent Variable: SR_Volts SR-Volts

                            Output Statistics

         Dep Var  Predicted   Std Error                                        Std Error  Student
  Obs    SR_Volts Value  Mean Predict    95% CL Mean      95% CL Predict   Residual  Residual Residual   -2-1 0 1 2

   1     0.1395   0.1286   0.002347   0.1238  0.1333   0.1071  0.1500   0.0109    0.0102    1.072           **
   2     0.1923   0.1952   0.001856   0.1915  0.1989   0.1739  0.2165  -0.002883  0.0103   -0.281
   3     0.2154   0.2198   0.001711   0.2164  0.2233   0.1986  0.2411  -0.004379  0.0103   -0.425
   4     0.3166   0.3289   0.001481   0.3260  0.3319   0.3077  0.3501  -0.0124    0.0103   -1.196      **
   5     0.3777   0.3786   0.001646   0.3753  0.3819   0.3574  0.3998  -0.000902  0.0103   -0.0875
   6     0.4479   0.4580   0.002154   0.4537  0.4623   0.4366  0.4794  -0.0101    0.0102   -0.987       *
   7     0.4748   0.4873   0.002386   0.4825  0.4921   0.4658  0.5088  -0.0125    0.0102   -1.231      **
   8     0.1391   0.1281   0.002351   0.1234  0.1329   0.1066  0.1496   0.0110    0.0102    1.081           **
   9     0.2065   0.2062   0.001788   0.2026  0.2098   0.1850  0.2275   0.000237  0.0103    0.0230
  10     0.2151   0.2211   0.001704   0.2177  0.2245   0.1999  0.2424  -0.005954  0.0103   -0.578       *
  11     0.3111   0.3209   0.001470   0.3179  0.3238   0.2997  0.3420  -0.009770  0.0103   -0.946       *
  12     0.3608   0.3718   0.001615   0.3686  0.3751   0.3506  0.3930  -0.0110    0.0103   -1.070      **
  13     0.4616   0.4644   0.002203   0.4599  0.4688   0.4429  0.4858  -0.002753  0.0102   -0.270
  14     0.4922   0.4932   0.002435   0.4883  0.4981   0.4717  0.5148  -0.000977  0.0101   -0.0963
  15     0.1779   0.1782   0.001970   0.1743  0.1822   0.1569  0.1996  -0.000327  0.0102   -0.0319
  16     0.2151   0.2190   0.001715   0.2155  0.2224   0.1977  0.2402  -0.003921  0.0103   -0.381
  17     0.3162   0.3272   0.001479   0.3243  0.3302   0.3061  0.3484  -0.0111    0.0103   -1.070      **
  18     0.3693   0.3782   0.001644   0.3749  0.3815   0.3569  0.3994  -0.008862  0.0103   -0.860       *
  19     0.4446   0.4550   0.002131   0.4507  0.4593   0.4336  0.4764  -0.0104    0.0102   -1.021      **
  20     0.4767   0.4911   0.002418   0.4862  0.4960   0.4696  0.5126  -0.0144    0.0102   -1.415      **
  21     0.2234   0.2228   0.001695   0.2194  0.2262   0.2016  0.2440   0.000560  0.0103    0.0544
  22     0.3344   0.3383   0.001500   0.3353  0.3413   0.3171  0.3595  -0.003890  0.0103   -0.377
  23     0.1389   0.1286   0.002347   0.1238  0.1333   0.1071  0.1500   0.0103    0.0102    1.013           **
  24     0.5676   0.5480   0.002910   0.5421  0.5538   0.5262  0.5698   0.0196    0.0100    1.953           ***
  25     0.1877   0.1820   0.001944   0.1781  0.1860   0.1607  0.2034   0.005660  0.0103    0.552            *
  26     0.4717   0.4661   0.002216   0.4616  0.4705   0.4446  0.4875   0.005669  0.0102    0.556            *
  27     0.2288   0.2253   0.001682   0.2220  0.2287   0.2041  0.2466   0.003496  0.0103    0.339
  28     0.1521   0.1281   0.002351   0.1234  0.1329   0.1066  0.1496   0.0239    0.0102    2.354           ****
  29     0.5755   0.5518   0.002944   0.5459  0.5577   0.5300  0.5736   0.0237    0.0100    2.364           ****
  30     0.1912   0.1927   0.001873   0.1889  0.1964   0.1714  0.2140  -0.001490  0.0103   -0.145


                 All Calibration Curves Combined      13:56 Thursday, October 5, 2006

                              The REG Procedure
                               Model: MODEL2
                     Dependent Variable: SR_Volts SR-Volts

                            Output Statistics

                                Cook's
                         Obs       D

                          1      0.031
                          2      0.001
                          3      0.002
                          4      0.015
                          5      0.000
                          6      0.022
                          7      0.042
                          8      0.031
                          9      0.000
                         10      0.005
                         11      0.009
                         12      0.014
                         13      0.002
                         14      0.000
                         15      0.000
                         16      0.002
                         17      0.012
                         18      0.009
                         19      0.023
                         20      0.057
                         21      0.000
                         22      0.001
                         23      0.027
                         24      0.161
```

```
          25    0.005
          26    0.007
          27    0.002
          28    0.148
          29    0.242
          30    0.000
```

All Calibration Curves Combined   13:56 Thursday, October 5, 2006

The REG Procedure
Model: MODEL2
Dependent Variable: SR_Volts SR-Volts

Output Statistics

Obs	Dep Var SR_Volts	Predicted Value	Std Error Mean Predict	95% CL Mean		95% CL Predict		Residual	Std Error Residual	Student Residual	-2-1 0 1 2
31	0.3569	0.3608	0.001570	0.3576	0.3639	0.3396	0.3820	-0.003864	0.0103	-0.375	
32	0.2282	0.2355	0.001632	0.2323	0.2388	0.2143	0.2568	-0.007344	0.0103	-0.712	*
33	0.3465	0.3506	0.001534	0.3475	0.3537	0.3294	0.3718	-0.004088	0.0103	-0.396	
34	0.1334	0.1281	0.002351	0.1234	0.1329	0.1066	0.1496	0.005257	0.0102	0.517	*
35	0.1749	0.1808	0.001952	0.1768	0.1847	0.1594	0.2021	-0.005837	0.0103	-0.569	*
36	0.5694	0.5459	0.002891	0.5401	0.5517	0.5241	0.5676	0.0235	0.0100	2.347	****
37	0.2293	0.2338	0.001640	0.2305	0.2371	0.2126	0.2551	-0.004562	0.0103	-0.443	
38	0.2052	0.2062	0.001788	0.2026	0.2098	0.1850	0.2275	-0.001023	0.0103	-0.0995	
39	0.1376	0.1281	0.002351	0.1234	0.1329	0.1066	0.1496	0.009424	0.0102	0.927	*
40	0.3506	0.3599	0.001567	0.3568	0.3631	0.3387	0.3811	-0.009335	0.0103	-0.905	*
41	0.5347	0.5459	0.002891	0.5401	0.5517	0.5241	0.5676	-0.0111	0.0100	-1.109	**
42	0.2277	0.2368	0.001626	0.2335	0.2401	0.2156	0.2580	-0.009085	0.0103	-0.881	*
43	0.3393	0.3468	0.001523	0.3437	0.3498	0.3256	0.3680	-0.007510	0.0103	-0.727	*
44	0.5580	0.5450	0.002883	0.5392	0.5508	0.5233	0.5668	0.0130	0.0100	1.298	**
45	0.1284	0.1281	0.002351	0.1234	0.1329	0.1066	0.1496	0.000303	0.0102	0.0298	
46	0.1780	0.1854	0.001921	0.1816	0.1893	0.1641	0.2068	-0.007394	0.0103	-0.721	*
47	0.2270	0.2304	0.001656	0.2271	0.2338	0.2092	0.2517	-0.003473	0.0103	-0.337	
48	0.1424	0.1281	0.002351	0.1234	0.1329	0.1066	0.1496	0.0142	0.0102	1.401	**
49	0.5738	0.5505	0.002933	0.5446	0.5564	0.5288	0.5723	0.0233	0.0100	2.326	****
50	0.3450	0.3472	0.001524	0.3441	0.3502	0.3260	0.3684	-0.002193	0.0103	-0.212	
51	0.1742	0.1736	0.002003	0.1695	0.1776	0.1522	0.1949	0.000681	0.0102	0.0665	

Output Statistics

Obs	Cook's D
31	0.002
32	0.006
33	0.002

All Calibration Curves Combined   13:56 Thursday, October 5, 2006

The REG Procedure
Model: MODEL2
Dependent Variable: SR_Volts SR-Volts

Output Statistics

Obs	Cook's D
34	0.007
35	0.006
36	0.229
37	0.002
38	0.000
39	0.023
40	0.009
41	0.051
42	0.010
43	0.006
44	0.070
45	0.000
46	0.009
47	0.001
48	0.052
49	0.232
50	0.000
51	0.000

```
Sum of Residuals                        0
Sum of Squared Residuals          0.00534
Predicted Residual SS (PRESS)     0.00601
```

APPENDIX B

Statistical Analysis for Cornmeal Experiments

Repeated Measures Analysis

```
Cornmeal Experiment                    15:50 Thursday, October 5, 2006    1

                           The Mixed Procedure

                            Model Information

              Data Set                     WORK.ONE
              Dependent Variable           voltage
              Covariance Structure         Unstructured
              Subject Effect               Vial
              Estimation Method            REML
              Residual Variance Method     None
              Fixed Effects SE Method      Model-Based
              Degrees of Freedom Method    Between-Within


                         Class Level Information

                 Class    Levels     Values

                 Vial        9       1 2 3 4 6 7 8 9 10
                 expt        3       1 2 3


                               Dimensions

                    Covariance Parameters          6
                    Columns in X                   4
                    Columns in Z                   0
                    Subjects                       9
                    Max Obs Per Subject            3
                    Observations Used             27
                    Observations Not Used          0
                    Total Observations            27



Cornmeal Experiment                    15:50 Thursday, October 5, 2006

                           The Mixed Procedure

                            Iteration History

        Iteration    Evaluations    -2 Res Log Like      Criterion

            0             1          -145.63569066
            1             1          -201.21368853      0.00000000


                        Convergence criteria met.


                      Estimated R Matrix for Vial 1

              Row        Col1         Col2         Col3
               1      0.000102     0.000100     0.000101
               2      0.000100     0.000105     0.000101
               3      0.000101     0.000101     0.000102


                       Estimated R Correlation
                         Matrix for Vial 1

              Row        Col1         Col2         Col3
```

```
1      1.0000      0.9683      0.9916
2      0.9683      1.0000      0.9694
3      0.9916      0.9694      1.0000
```

Covariance Parameter Estimates

Cov Parm	Subject	Estimate	Standard Error	Z Value	Pr Z
UN(1,1)	Vial	0.000102	0.000051	2.00	0.0228
UN(2,1)	Vial	0.000100	0.000051	1.97	0.0491

Cornmeal Experiment   15:50 Thursday, October 5, 2006

The Mixed Procedure

Covariance Parameter Estimates

Cov Parm	Subject	Estimate	Standard Error	Z Value	Pr Z
UN(2,2)	Vial	0.000105	0.000053	2.00	0.0228
UN(3,1)	Vial	0.000101	0.000051	1.99	0.0464
UN(3,2)	Vial	0.000101	0.000051	1.97	0.0490
UN(3,3)	Vial	0.000102	0.000051	2.00	0.0228

Fit Statistics

-2 Res Log Likelihood	-201.2
AIC (smaller is better)	-189.2
AICC (smaller is better)	-184.3
BIC (smaller is better)	-188.0

Null Model Likelihood Ratio Test

DF	Chi-Square	Pr > ChiSq
5	55.58	<.0001

Type 3 Tests of Fixed Effects

Effect	Num DF	Den DF	F Value	Pr > F
expt	2	8	1.48	0.2836

Cornmeal Experiment   15:50 Thursday, October 5, 2006

The Mixed Procedure

Least Squares Means

Effect	expt	Estimate	Standard Error	DF	t Value	Pr > |t|
expt	1	0.2159	0.003358	8	64.28	<.0001
expt	2	0.2155	0.003417	8	63.07	<.0001
expt	3	0.2151	0.003374	8	63.76	<.0001

Differences of Least Squares Means

Effect	expt	expt	Estimate	Standard Error	DF	t Value	Pr > |t|
expt	1	2	0.000360	0.000855	8	0.42	0.6850
expt	1	3	0.000752	0.000437	8	1.72	0.1239
expt	2	3	0.000392	0.000841	8	0.47	0.6533

```
Cornmeal Experiment                        15:50 Thursday, October 5, 2006

                            The MEANS Procedure

                      Analysis Variable : voltage voltage

             N
expt        Obs       N        Mean        Std Dev       Minimum       Maximum
ƒƒƒƒƒƒƒƒƒƒƒƒƒƒƒƒƒƒƒƒƒƒƒƒƒƒƒƒƒƒƒƒƒƒƒƒƒƒƒƒƒƒƒƒƒƒƒƒƒƒƒƒƒƒƒƒƒƒƒƒƒƒƒƒƒƒƒƒƒƒƒƒƒƒƒƒƒ
  1          9       9      0.2158745     0.0100749     0.1963265     0.2276019

  2          9       9      0.2155146     0.0102510     0.1960725     0.2263038

  3          9       9      0.2151225     0.0101215     0.1965956     0.2280450
ƒƒƒƒƒƒƒƒƒƒƒƒƒƒƒƒƒƒƒƒƒƒƒƒƒƒƒƒƒƒƒƒƒƒƒƒƒƒƒƒƒƒƒƒƒƒƒƒƒƒƒƒƒƒƒƒƒƒƒƒƒƒƒƒƒƒƒƒƒƒƒƒƒƒƒƒƒ
```
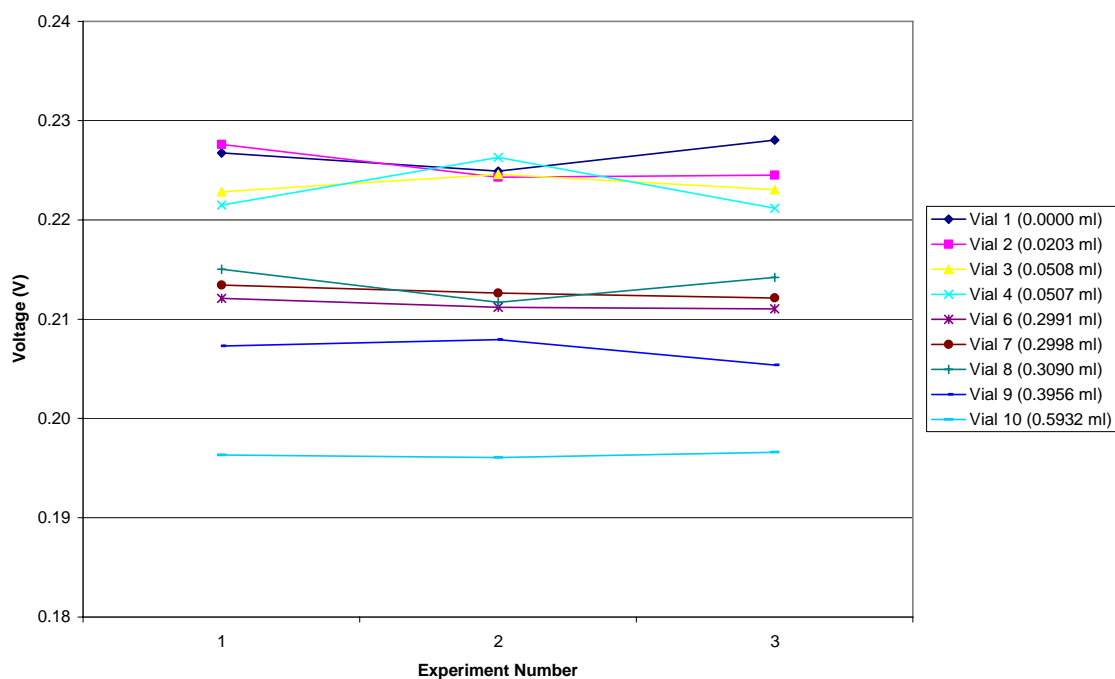

Figure B.1: Graph showing repeated measurements on test vials

Regression Analysis
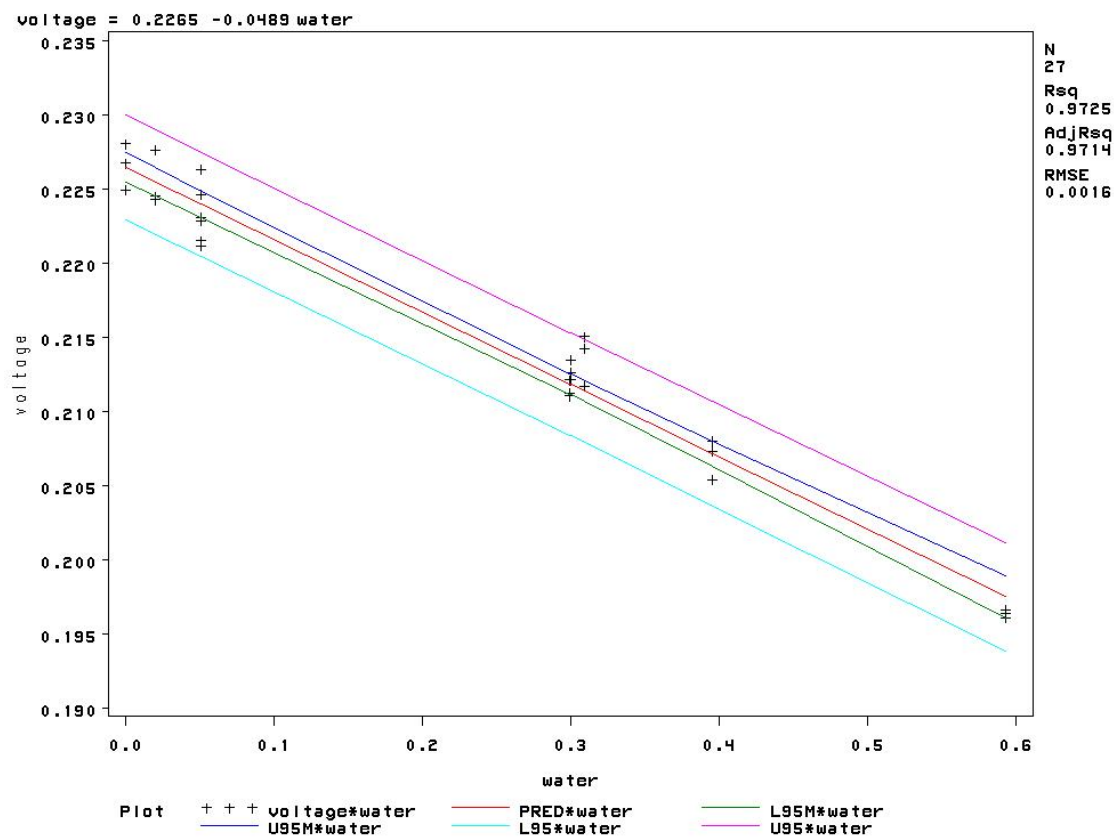
Figure B.2: Output voltage vs. water content

```
                          test dump                    15:52 Thursday, October 5, 2006

        Obs     expt    Vial     water      voltage      sr_voltage

         1       1       1      0.0000     0.22673       0.47616
         2       1       2      0.0203     0.22760       0.47708
         3       1       3      0.0508     0.22284       0.47206
         4       1       4      0.0507     0.22150       0.47063
         5       1       6      0.2991     0.21211       0.46055
         6       1       7      0.2998     0.21345       0.46201
         7       1       8      0.3090     0.21503       0.46372
         8       1       9      0.3956     0.20729       0.45529
         9       1      10      0.5932     0.19633       0.44309
        10       2       1      0.0000     0.22491       0.47425
        11       2       2      0.0203     0.22428       0.47358
        12       2       3      0.0508     0.22460       0.47392
        13       2       4      0.0507     0.22630       0.47571
        14       2       6      0.2991     0.21121       0.45958
        15       2       7      0.2998     0.21261       0.46110
        16       2       8      0.3090     0.21168       0.46009
        17       2       9      0.3956     0.20796       0.45603
        18       2      10      0.5932     0.19607       0.44280
        19       3       1      0.0000     0.22805       0.47754
        20       3       2      0.0203     0.22450       0.47382
        21       3       3      0.0508     0.22305       0.47228
        22       3       4      0.0507     0.22118       0.47029
        23       3       6      0.2991     0.21103       0.45938
        24       3       7      0.2998     0.21212       0.46056
        25       3       8      0.3090     0.21421       0.46283
        26       3       9      0.3956     0.20536       0.45317
        27       3      10      0.5932     0.19660       0.44339
```

```
                    All Cornmeal Experiments Combined      15:52 Thursday, October 5, 2006

                                 The REG Procedure
                                  Model: MODEL1
                          Dependent Variable: voltage voltage
```

```
                              Analysis of Variance

                                        Sum of          Mean
        Source              DF         Squares        Square   F Value   Pr > F

        Model                1         0.00241       0.00241    884.45   <.0001
        Error               25      0.00006803    0.00000272
        Corrected Total     26         0.00247


                    Root MSE             0.00165    R-Square     0.9725
                    Dependent Mean       0.21550    Adj R-Sq     0.9714
                    Coeff Var            0.76546


                              Parameter Estimates

                                     Parameter      Standard
        Variable    Label      DF     Estimate         Error   t Value   Pr > |t|

        Intercept   Intercept   1      0.22646    0.00048636    465.62    <.0001
        water       water       1     -0.04886       0.00164    -29.74    <.0001
```

All Cornmeal Experiments Combined   15:52 Thursday, October 5, 2006

The REG Procedure
Model: MODEL1
Dependent Variable: voltage voltage

Output Statistics

```
       Dep Var  Predicted     Std Error                                             Std Error   Student
Obs    voltage      Value  Mean Predict    95% CL Mean       95% CL Predict  Residual  Residual  Residual   -2-1 0 1 2

 1     0.2267     0.2265      0.000486   0.2255   0.2275   0.2229   0.2300   0.000268   0.00158    0.170    |       |
 2     0.2276     0.2255      0.000462   0.2245   0.2264   0.2219   0.2290   0.002132   0.00158    1.346    |    ** |
 3     0.2228     0.2240      0.000427   0.2231   0.2249   0.2205   0.2275  -0.001144   0.00159   -0.718    |  *    |
 4     0.2215     0.2240      0.000427   0.2231   0.2249   0.2205   0.2275  -0.002489   0.00159   -1.562    |***    |
 5     0.2121     0.2118      0.000340   0.2111   0.2125   0.2084   0.2153   0.000260   0.00161    0.161    |       |
 6     0.2134     0.2118      0.000341   0.2111   0.2125   0.2083   0.2153   0.001636   0.00161    1.014    |    ** |
 7     0.2150     0.2114      0.000347   0.2107   0.2121   0.2079   0.2148   0.003668   0.00161    2.274    |    ****|
 8     0.2073     0.2071      0.000424   0.2063   0.2080   0.2036   0.2106   0.000157   0.00159    0.0983   |       |
 9     0.1963     0.1975      0.000684   0.1961   0.1989   0.1938   0.2012  -0.001152   0.00150   -0.768    |  *    |
10     0.2249     0.2265      0.000486   0.2255   0.2275   0.2229   0.2300  -0.001552   0.00158   -0.985    |  *    |
11     0.2243     0.2255      0.000462   0.2245   0.2264   0.2219   0.2290  -0.001192   0.00158   -0.752    |  *    |
12     0.2246     0.2240      0.000427   0.2231   0.2249   0.2205   0.2275   0.000619   0.00159    0.389    |       |
13     0.2263     0.2240      0.000427   0.2231   0.2249   0.2205   0.2275   0.002319   0.00159    1.455    |    ** |
14     0.2112     0.2118      0.000340   0.2111   0.2125   0.2084   0.2153  -0.000636   0.00161   -0.394    |       |
15     0.2126     0.2118      0.000341   0.2111   0.2125   0.2083   0.2153   0.000700   0.00161    0.495    |       |
16     0.2117     0.2114      0.000347   0.2107   0.2121   0.2079   0.2148   0.000317   0.00161    0.196    |       |
17     0.2080     0.2071      0.000424   0.2063   0.2080   0.2036   0.2106   0.000829   0.00159    0.520    |  *    |
18     0.1961     0.1975      0.000684   0.1961   0.1989   0.1938   0.2012  -0.001406   0.00150   -0.937    |  *    |
19     0.2280     0.2265      0.000486   0.2255   0.2275   0.2229   0.2300   0.001583   0.00158    1.004    |    ** |
20     0.2245     0.2255      0.000462   0.2245   0.2264   0.2219   0.2290  -0.000968   0.00158   -0.611    |  *    |
21     0.2231     0.2240      0.000427   0.2231   0.2249   0.2205   0.2275  -0.000928   0.00159   -0.582    |  *    |
22     0.2212     0.2240      0.000427   0.2231   0.2249   0.2205   0.2275  -0.002807   0.00159   -1.762    |***    |
23     0.2110     0.2118      0.000340   0.2111   0.2125   0.2084   0.2153  -0.000814   0.00161   -0.504    |  *    |
24     0.2121     0.2118      0.000341   0.2111   0.2125   0.2083   0.2153   0.000305   0.00161    0.189    |       |
25     0.2142     0.2114      0.000347   0.2107   0.2121   0.2079   0.2148   0.002848   0.00161    1.766    |    ***|
26     0.2054     0.2071      0.000424   0.2063   0.2080   0.2036   0.2106  -0.001769   0.00159   -1.110    | **    |
27     0.1966     0.1975      0.000684   0.1961   0.1989   0.1938   0.2012  -0.000883   0.00150   -0.588    |  *    |
```

All Cornmeal Experiments Combined   15:52 Thursday, October 5, 2006

The REG Procedure
Model: MODEL1
Dependent Variable: voltage voltage

Output Statistics

```
              Cook's
       Obs       D

         1     0.001
         2     0.077
         3     0.018
         4     0.088
         5     0.001
         6     0.023
         7     0.119
         8     0.000
         9     0.061
        10     0.046
        11     0.024
        12     0.005
        13     0.076
        14     0.003
        15     0.005
        16     0.001
        17     0.010
        18     0.091
        19     0.048
        20     0.016
        21     0.012
        22     0.111
        23     0.006
        24     0.001
        25     0.072
        26     0.044
        27     0.036
```

All Cornmeal Experiments Combined   15:52 Thursday, October 5, 2006

The REG Procedure
Model: MODEL1
Dependent Variable: voltage voltage

Sum of Residuals   0
Sum of Squared Residuals   0.00006803
Predicted Residual SS (PRESS)   0.00007842

BIBLIOGRAPHY

[1]   F. T. Ulaby, R. K. Moore and A. K. Fung, *Microwave Remote Sensing : Fundamentals and Radiometry.* , vol. 1, Reading, Mass.: Addison-Wesley Pub. Co., Advanced Book Program/World Science Division, 1981, pp. 456.

[2]   W. J. Yang, S. Mochizuki and P. T. Yang, "Applications of Microwave Radiation in Medicine," *J Mech Med Biol,* vol. 2, pp. 53-63, Oct. 2002.

[3]   N. Skou, *Microwave Radiometer Systems--Design and Analysis.* Norwood, MA: Artech House, 1989, pp. 162.

[4]   A. Rosen, M. A. Stuchly and A. V. Vorst, "Applications of RF/microwaves in medicine," *IEEE Trans. Microwave Theory Tech.,* vol. 50, pp. 963-974, 2002.

[5]   E. A. Cheever and K. R. Foster, "Microwave radiometry in living tissue: what does it measure?" *IEEE Trans. Biomed. Eng.,* vol. 39, pp. 563-568, Jun. 1992.

[6]   T. Sugiura, Y. Kouno, A. Hashizume, H. Hirata, J. W. Hand, Y. Okita and S. Mizushina, "Five-band microwave radiometer system for non-invasive measurement of brain temperature in new-born infants: System calibration and its feasibility," in *Conference Proceedings - 26th Annual International Conference of the IEEE Engineering in Medicine and Biology Society, EMBC 2004, Sep 1-5 2004,* 2004, pp. 2292-2295.

[7]   F. Bardati, G. Marrocco and P. Tognolatti, "Time-Dependent Microwave Radiometry for Measurement of Temperature in Medical Applications," *IEEE Transactions on Microwave Theory and Techniques,* vol. 52, pp. 1917-1924, Aug. 2004.

[8]   R. Klabunde, "Cardiovascular physiological concepts," Aug. 29, 2005. Accessed Oct. 4, 2006. Available: http://www.cvphysiology.com/CAD/CAD005.htm

[9]   "Diabetes statistics," American Diabetes Association, Accessed Sept. 26, 2006. Available: http://www.diabetes.org/diabetes-statistics.jsp

[10] J. A. Tamada, M. Lesho and M. J. Tierney, "Keeping Watch On Glucose," *IEEE Spectrum,* pp. 52-57, April. 2002.

[11] United States, "United States Frequency Allocations," Washington, DC: U.S. Dept. of Commerce, National Telecommunications and Information Administration, Office of Spectrum Management, 2003.

[12] F. P. Incropera and D. P. DeWitt, *Fundamentals of Heat and Mass Transfer.* ,5th ed. New York: J. Wiley, 2002, pp. 981.

[13] L. C. Shen and J. A. Kong, *Applied Electromagnetism.* ,3rd ed.Boston: PWS Pub. Co., 1995, pp. 606.

[14] D. M. Pozar, *Microwave Engineering.* 3rd ed. Hoboken, NJ: J. Wiley, 2005, pp. 700.

[15] F. T. Ulaby, R. K. Moore and A. K. Fung, *Microwave Remote Sensing : Active and Passive : 3 : From Theory to Applications.* vol. 4, Dedham: Artech House, 1986.

[16] F. T. Ulaby, R. K. Moore and A. K. Fung, *Microwave Remote Sensing Active and Passive Radar Remote Sensing and Surface Scattering and Emission Theory.* vol. II, Reading, MA: Addison-Wesley, 1982, pp. 607.

[17] Millitech. "Microwave and millimeter wave radiometry," Accessed June 12, 2006, pp. 10. Available: http://www.millitech.com/pdfs/Radiometer.pdf

[18] A. Colliander, "Noise Injection Radiometer Test Specifications and Requirements," pp. 7., Sept. 2002.

[19] G. Leinweber, "Square Law Diode Detectors in 50 Ohm Systems," vol. 2006, pp. 3, May. 2001.

[20] N. Skou and D. Le Vine, *Microwave Radiometer Systems Design and Analysis: Second Edition.* ,2nd ed. Norwood, MA: Artech House, 2006, pp. 222.

[21] "Water," Wikimedia Foundation Inc., Sept. 20, 2006. Accessed Sept. 20, 2006, Available: http://en.wikipedia.org/wiki/Water

[22] N. K. Gupta, S. K. Srivastava and H. V. Tiwari, "Estimation of Emissivity Characteristics of Biological Tissues at Microwave Frequency," *IE(I) Journal-ID,* vol. 84, pp. 1-3, 2004.

[23] S. Gabriel, R. W. Lau and C. Gabriel, "The dielectric properties of biological tissues: III. Parametric models for the dielectric spectrum of tissues," *Phys. Med. Biol.,* vol. 41, pp. 2271-2293, Nov. 1996.

[24] S. S. Seker, G. Apaydin and M. Kuzu, "Comparison of Electrical Parameters of Human Body Parts with Vegetation," vol. 4, pp. 3241-3244, 2003.

[25] "Permittivity," Wikimedia Foundation, Inc., Sept. 8, 2006. Accessed Sept. 21, 2006, Available: http://en.wikipedia.org/wiki/Permittivity

[26] O. G. Martinsen, S. Grimnes and H. P. Schwan, "Interface phenomena and dielectric properties of biological tissue," in *Encyclopedia of Surface and Colloid Science* Anonymous Marcel Dekker, Inc., 2002, pp. 2643-2652.

[27] E. C. Green, "Design of a microwave sensor for non-invasive determination of blood-glucose concentration." Master's thesis, Baylor University, 2004.

[28] R. Pethig, "Dielectric properties of body tissues," *Clinical Physics and Physiological Measurement : An Official Journal of the Hospital Physicists' Association, Deutsche Gesellschaft Für Medizinische Physik and the European Federation of Organisations for. Medical Physics,* vol. 8 Suppl A, pp. 5-12, 1987.

[29] C. M. Alabaster and P. J. S. Dahele, "The Microwave Properties of Tissue and Other Lossy Dielectrics," Cranfield University; College of Defence Technology; Department of Aerospace, Power and Sensors, July 1, 2004.

[30] T. J. Jackson. "Description of soil moisture retrieval algorithm for ADEOS II AMSR," Accessed June 15, 2006, pp. 6. Available: http://sharaku.eorc.jaxa.jp/AMSR/doc/alg/14_alg.pdf

[31] Y. Nikawa and D. Someya, "Non-invasive measurement of blood sugar level by millimeter waves," *Microwave Symposium Digest 2001 IEEE MTT-S International,* vol. 1, pp. 171-174, May. 2001.

[32] J. H. Park, C. S. Kim, B. C. Choi and K. Y. Ham, "The correlation of the complex dielectric constant and blood glucose at low frequency," *Biosens. Bioelectron.,* vol. 19, pp. 321-324, Dec 15. 2003.

[33] J. C. Lantis 2nd, K. L. Carr, R. Grabowy, R. J. Connolly and S. D. Schwaitzberg, "Microwave applications in clinical medicine," *Surg. Endosc.,* vol. 12, pp. 170-176, Feb. 1998.

[34] A. H. Barrett and P. C. Myers, "Subcutaneous temperatures: a method of noninvasive sensing," *Science,* vol. 190, pp. 669-671, Nov 14. 1975.

[35] K. Schneeberger, C. Stamm, C. Matzler and H. Fluhler, "Ground-based dual-frequency radiometry of bare soil at high temporal resolution," *IEEE Trans. Geosci. Remote Sens.,* vol. 42, pp. 588-595, 2004.

[36] J. Wang, J. Shiue and E. Engman, *Remote Measurements of Soil Moisture by Microwave Radiometers at BARC Test Site.* , vol. 80720, Baltimore: N.A.S.A., 1980, pp. 113.

[37] V. Seshiah and C. V. Harinarayan, "Insulin Kinetics," *INT. J. DIAB. DEV. COUNTRIES,* vol. 18, pp. 19-22, 1998.